MICHIGAN STATE UNIVERSITY

CYCLOTRON LABORATORY

$\ell = 0$, SPIN-FLIP EXCITATIONS IN (p,n) AND (p,p′) REACTIONS

A. GALONSKY, N. ANANTARAMAN, G.M. CRAWLEY,
C. DIJALALI, N. MARTY, M. MORLET, A. WILLIS
and J.C. JOURDAIN

FEBRUARY 1984

MSUCL-450

MSUCL-450
February 1984

Lecture given at the 15th Summer School on
Nuclear Physics at Mikolajki, Poland,
September 5-17, 1983

ℓ=0, Spin-Flip Excitations in (p,n) and (p,p') Reactions

A. Galonsky,* N. Anantaraman* and G.M. Crawley*

Cyclotron Laboratory, Michigan State University
East Lansing, Michigan 48824, U.S.A.

and

C. Djalali, N. Marty, M. Morlet, A. Willis and J.C. Jourdain
Institut de Physique Nucleaire, BP n° 1, 91406 Orsay, France

Abstract

The evidence for ℓ=0, isovector, spin-flip strength in (p,n) reactions (Gamow-Teller strength) and in the corresponding (p,p') reactions is reviewed.

*Supported by the National Science Foundation under Grants PHY-80-17605, INT-81-16064 and INT-82-13242.

I. Introduction

The study of simple states at high excitation, that is, the study of giant resonances, has taught us much about the structure of nuclei. If we think of such a state as a one particle-one hole (1p-1h) configuration, that configuration will be most easily detected if it is conferred on one state or on a group of close-lying states. Even then, it may be lost in a sea of complex (np-nh) states, unless a suitably selective probe is used to excite it. Starting with the electric dipole resonance, some properties of four electric giant resonances have been established with probes consisting of photon absorption and inelastic scattering of protons, deuterons, and alpha particles.

This paper deals with magnetic, or spin, excitations by direct reactions of high-energy (~100-200 MeV) protons in which there is a transfer of one unit of spin, one unit of isospin, but no orbital angular momentum to the nucleus. Spin flip without isospin-flip also occurs, and a little can be said about a strength concentration of such excitations. The small-angle selectivity for ℓ=0 transfers is an essential part of the experimental technique. In this domain the central force part of the effective nucleon-nucleon interaction is dominant, that is, the tensor and $\vec{L}\cdot\vec{S}$ parts can usually be neglected to good approximation.

II. (p,n) Reactions

Only the isospin-dependent part of the central force can induce a (p,n) transition. When this is done without a

spin flip, a neutron in the target nucleus is converted to a proton, but no other quantum number of the nucleon is changed. Formally, we say that the isospin lowering operator t_- has flipped the isospin of a target nucleon from $t_z=+1/2$ to $t_z=-1/2$. This is the transition to the isobaric analog state (IAS) discovered by Anderson and Wong.[1] In a further study of IAS Doering et al.[2] found a broad bump near the IAS in the ^{90}Zr(p,n) reaction at 35 and 45 MeV. From its energy and angular distribution they concluded that they had observed a $0^+ \rightarrow 1^+$ transition. Hence, one unit of isospin and one unit of spin were exchanged; the orbital angular momentum transferred could be 0 or 2 units, but was dominated at small angles by $\ell=0$. For the IAS transition, $0^+ \rightarrow 0^+$, only $\ell=0$ is possible. These features are shown in Fig. 1. The broad 1^+ peak arises from a final configuration $(\nu g_{9/2}^{-1} \pi g_{7/2})1^+$, an obvious spin flip, and the narrow peak at lower excitation from $(\nu g_{9/2}^{-1} \pi g_{9/2})1^+$. The 0^+ configuration is $(\nu g_{9/2}^{-1} \pi g_{9/2})0^+$. The additional labelling, F and GT, means Fermi and Gamow-Teller. The operators, t_- and $\sigma_\mu t_-$, inducing these (p,n) transitions are the same as in Fermi and Gamow-Teller β decay. The magnitudes of the F and broad GT peaks warrant the terms Fermi and Gamow-Teller giant resonances. On the basis of charge independence the giant GT resonance was predicted[3] before it was observed.

The development of a neutron time-of-flight system[4] and of large neutron detectors[5,6] at the Indiana University Cyclotron Facility led to the main point of this talk

through a broad investigation[7-9] of the giant GT resonance. The work was aided by the higher proton energies at Indiana and the circumstance that the ratio of the spin-flip to the non-flip force, $V_{\sigma t}/V_t$, increases with energy,[10,11] thus enhancing measurement of GT strength. To illustrate this point, compare the GT peaks at 80, 120 and 160 MeV in Fig. 2 with those in Fig. 1. At 120 and 160 MeV the F resonance is much weaker than the giant GT resonance. It is also fortunate that (p,n) reactions can be done at 0° because, particularly at Indiana energies, the forward direction is very selective of transitions having $\ell=0$. An example of this selectivity may be seen in Fig. 3. The F and GT peaks which are so dominant at 0° are barely visible beyond 8.2°. The peak at higher excitation energy, $E_n \simeq 93$ MeV, results from $\ell=1$ and it peaks near 6°.

The fact that the work at Indiana by Goodman, Rapaport, Gaarde, Taddeucci, et al. has shown the GT resonance to be a universal property of nuclei is of fundamental significance. But the concentration of strength in a giant resonance is meaningful only in relation to a sum rule. For Fermi β^- decay we have[9,12]

$$S = \sum_f \left| \langle f | \sum_{k=1}^{A} t_-(k) | i \rangle \right|^2 = N - Z \qquad (1)$$

and for GT decay

$$S(\beta^-) - S(\beta^+) = \sum_f \sum_\mu \left| \langle f | \sum_{k=1}^{A} \sigma_\mu(k) t_-(k) | i \rangle \right|^2 - \sum_{f'} \sum_\mu \left| \langle f' | \sum_{k=1}^{A} \sigma_\mu(k) t_+(k) | i \rangle \right|^2 = 3(N-Z) \qquad (2)$$

These are model-independent sum rules. For GT β^- decay the rule only puts a lower limit on the strength. Except in certain light nuclei these rules cannot be tested. Fermi decay goes entirely to the IAS, which is energetically inaccessible for nuclei with a neutron excess. The same is true for GT β^- decay, and for GT β^+ decay there is little or no strength in the decay of the ground state; that is what the giant GT resonance tells us. In $^{90}Nb \xrightarrow{\beta^+} {}^{90}Zr$ Figs. 1-3 show that the strength is mostly in the 5-10 MeV range of excitation in ^{90}Nb. Because the $0^+ \to 1^+$ (p,n) operator, in the small-angle, or low-momentum transfer, regime is almost the same as the GT operator, we can deduce a GT strength from a small-angle (p,n) cross section from[13]

$$\sigma_{GT}(0^\circ) \sim N^D J_{\sigma\tau}^2 \langle GT \rangle^2 . \qquad (3)$$

In this relation N^D accounts for the Coulomb-nuclear distortion of the ingoing and outgoing waves, $J_{\sigma\tau}$ is the volume integral of the spin-isospin central part of the effective interaction, and $\langle GT \rangle^2$ is the square of a GT matrix to a particular final state on a sum to various final states, as in (1) and (2). There are two good ways[7,9,11] to calibrate (3) so that $\langle GT \rangle^2$ can be obtained from a measurement of $\sigma_{GT}(0^\circ)$. Each method involves application of (3) to specific transitions where the matrix element is known and $N^D J^2_{\sigma\tau}$ can be determined. Then $\langle GT \rangle^2$ can be determined for all of the GT cross section observed in the (p,n) reaction.

Some of the representative results[9] are given in Fig. 4. Use of the sum rule (2) is possible because Pauli blocking makes $S(\beta^+) \simeq 0$ in heavy nuclei; specific estimates of $S(\beta^+)$ are made in each case. The inescapable conclusion is that roughly 50% - 60% of the possible strength is revealed in (p,n) spectra. The exact amount depends on the treatment of the continuum background[14], particularly at higher excitation.[15,16] The most popular explanation[17] of the missing strength involves mixing Δ-hole configurations with the proton-hole configurations we have been discussing. The mixing is small, but the Δ strength is much greater than 3(N-Z) because there is no Pauli blocking; every neutron can make a spin-isospin transition to a Δ. Furthermore, the interaction being repulsive results in a decrease in strength at the lower energy, ~10 MeV, and of course, a relatively small increase at the Δ-hole energy 300 MeV. The Δ-hole region is not accessible at Indiana energies. Before the GT resonance was discovered a (p,n) experiment was performed at 0° with 800 MeV protons.[18] The spectrum, Fig. 5, clearly shows a broad peak centered at 300 meV. The origin is probably a quasi-free charge exchange scattering. A recently reported $^{12}C(^3He,t)$ experiment[19] has the same feature and many have the same explanation. In any case it should be noted that an allowed beta decay has $\ell=0$; when $qR \gtrsim 1$ (q = momentum transfer $\div \hbar$ and R = nuclear radius), we can have $\ell \geq 1$. In the (p,n) experiment[18] $qR \sim 4$.

III. Inelastic Scattering

The progress made in understanding GT β decay in heavy nuclei by means of the (p,n) reaction illustrates the value of studying a problem from more than one viewpoint. Because we are necessarily dealing with an isovector transition in the (p,n) reaction, where $\Delta t_z = -1$, there are related final states in the target, where $\Delta t_z = 0$. The relationship is shown schematically in Fig. 6 where one sees that in the parent nucleus the 1^+, T_o state can be excited both by electromagnetic interactions and by (p,p'). In the (p,n) reaction the analogue of the 1^+, T_o state is populated, but the bulk of the strength goes to the anti-analogue 1^+, (T_o-1) state. In fact, if one looks carefully at the 0.1^o and 4.1^o spectra in Fig. 3, one can see the T_o component on the left hand tail of the giant GT (T_o-1 component) resonance. A better view of a T_o component is in the ^{48}Ca(p,n) reaction performed by the Kent State group. A spectrum from their work[20] is reproduced in Fig. 7; the T_o (=4) component stands alone at 16.8 MeV excitation in ^{48}Sc. Since T_o states are direct analogues of states in the target, they should be seen in (e,e') and (p,p') if these reactions can be used in a suitably selective manner.

Backward scattering of electrons enhances the detection of magnetic transitions.[21] For Ml transitions the operator may be written as a sum of isoscalar and isovector terms as

$$\sum_{k=1}^{A} \left\{ \left[g_k \frac{\vec{l}}{2} + \left(\frac{g_k+g_n}{2}\right)\vec{s} \right] - \left[g_k \frac{\vec{l}}{2} + \left(\frac{g_k-g_n}{2}\right)\vec{s} \right](2t_z) \right\} \quad (4)$$

Because of the values of g_p (5.59 μ_N) and g_n (-3.83 μ_N), the isovector term dominates this expression. Thus for those cases where there is a pure neutron excitation, the orbital term disappears and the Ml operator also reduces to a $\sigma\tau$ term. For those cases, and only for those cases, should there be a close comparison between the relative strengths observed in (e,e'), (p,n) and (p,p'). This is the reason why one often speaks loosely of 1^+ spin-flip transitions as Ml transitions. For other cases, where both proton and neutron excitations contribute, there may be differences in detail between the results with the different probes.

In the case of ^{90}Zr the Ml transition should be predominantly a neutron $g_{9/2} \rightarrow g_{7/2}$ excitation and, because of the strong (p,n) transition to the daughter 1^+ state, should also be strong. Furthermore, if the identification of the T_o peak in (p,n) is correct, the excitation energy in ^{90}Zr should be the same as the T_o, IAS separation in Fig. 3, i.e., 8-9 MeV. In an (e,e') experiment[22] three definite 1^+ states were found, including one at 9.00 MeV.

Finally, the same states should be excited in (p,p'). In an experiment at 24 MeV no 1^+ states were seen.[23] We now understand that (p,p'), even at small angles, is not a sufficiently selective probe of isovector 1^+ states at 24 MeV. Only with $\sigma\tau$ dominance at higher energies[10,11] is it effective. The first example[24] in which the Ml excitation was seen in (p,p') was in ^{90}Zr and then[25] in ^{90}Zr, ^{94}Zr and ^{96}Zr, as shown in Fig. 7a. This work was done with the 201

MeV proton beam of the Orsay synchrocyclotron coupled with the highly developed detection system of the spectrometer magnet[26], which allowed (p,p') measurements at laboratory angles as small as 3°. In ^{90}Zr a bump similar to that shown here was also observed at TRIUMF[27], and in a recent experiment[28] at LAMPF with 319 MeV protons, cross sections, analyzing powers, and spin-flip probabilities were measured. Comparison with the (e,e') work is not too satifactory because (e,e') sees sharp states, not a bump. The fine structure in the bump was studied carefully with 60 keV resolution in the LAMPF experiment, but there was only partial agreement with the (e,e') structure.

The angular distributions obtained in the Orsay experiment are shown in Fig. 8. They are very sharply forward peaked and agree with those predicted from DWBA calculations and with the measured (p,n) angular distribution to the 1^+, (T_o-1) G-T state at the same bombarding energy. The angular distribution also matches closely the $\Delta L=0$ angular distribution for a known 1^+ state in ^{40}Ca. If the angular momentum transfer is indeed zero, this implies that the spin-parity is of course 0^+ or 1^+. If the state were 0^+, there would be no obvious reason why it should not have been seen at lower proton bombarding energy. However, the relative increase in strength of the $V_{\sigma\tau}$ term explains the strong enhancement of a 1^+ state. The strength observed is reasonably consistent

with that observed in the (p,n) reaction. Finally, the spin-flip measurements[28] confirm the 1^+ assignment. The curves shown in Fig. 8 were computed with the codes DWBA 70[29] and RESEDA[30] using wave functions derived from shell model calculations.[31] Each program uses phase shifts obtained from free nucleon-nucleon scattering, but DWBA 70 requires input in terms of the parameters of an effective interaction. It also results in division of the scattering into direct and exchange parts. The parameterization of Love and Franey[10] was used. If the approximations used in each treatment are good, the results should agree, and as we see in Fig. 8, they are similar but not identical. For each code the same scaling factor, 0.26, was used to fit the ^{90}Zr data. This number is about the same as the fraction of the predicted B(M1) strength observed in the (e,e') experiment[22] and about half the quenching factor observed (Fig. 4) in (p,n) for the Gamow-Teller strength.

By this time we have searched for ℓ=0, spin-flip strength via (p,p') at Orsay in 29 nuclei from ^{24}Mg to ^{208}Pb. Some of the spectra for Mo isotopes are shown in Fig. 9, for ^{51}V in Fig. 10, for other N=28 nuclei in Fig. 11, and for Ni isotopes in Fig. 12. For the first seventeen targets we studied[31] a summary of some characteristics of the resonance and the ratio of experimental to theoretical predicted cross sections (Q) is given in Table 1. The calculations were all done using the code RESEDA with the Paris potential. Q appears to be constant with mass number. Each

Mo spectrum is broad and structured as in the Zr spectra. In all cases either a broad feature or individual levels with very peaked angular distributions were observed. The sharpness of the angular distribution is demonstrated in Fig. 10 which shows two spectra from ^{51}V. The prominent peak seen clearly at 3^{o} has practically disappeared by 8^{o}.

The excitation energies of the structures observed remain rather constant as a function of mass, which is not too surprising for an M1 transition. The excitation energy depends on the spin-orbit splitting plus a residual particle-hole interaction, both of which do not change greatly with A. This is expressed more quantitatively in the calculation of Bertsch[32] which matches the observed excitation energies quite well.

For other N=28 nuclei - ^{48}Ca, ^{50}Ti, ^{52}Cr, and ^{54}Fe - spectra taken at 3^{o} are shown in Fig. 11. For all the targets, nearly all the states observed at small angles between 8 and 15 MeV excitation energy have a forward peaked angular distribution well fitted by a $\Delta L = 0$ shape. As one adds protons to ^{48}Ca in moving to ^{54}Fe, the simple state at 10.2 MeV excitation energy in ^{48}Ca, which presumably arises mainly from the neutron excitation with the configuration $\{f_{7/2}^{-1}, f_{5/2}\}^{1+}$, splits up into a number of different states. In ^{50}Ti, this neutron excitation is still visible as a cluster of states whose centroid is very close to the centroid of the simple state in ^{48}Ca. Also visible in ^{50}Ti is a further cluster of states near 8.5 MeV excitation

energy, which are predicted by the model of Metsch and Knupfer[33] to arise mainly from proton excitations with the same configuration $\{f_{7/2}^{-1}, f_{5/2}\}^{1+}$. However, for ^{52}Cr and ^{54}Fe, the strength is spread more widely between 8 and 12 MeV excitation energy and it is no longer possible to divide the states into neutron and proton excitations. Examples of angular distributions for some individual states in ^{50}Ti are shown in Fig. 13. Within the experimental errors they are all identical. This shape is well reproduced by the angular distribution computed for a strong model state at 13.00 MeV which is excited by a pure isovector interaction. The model[33] might not assign individual strengths correctly, but the summed strength should be more reliable. We see, however, in Fig. 13 that the theory overpredicts by a factor of four -- another example of spin-flip quenching. The quenching factors in ^{52}Cr and ^{54}Fe with the same model[33] are 0.36 and 0.35, respectively. The distribution of 1^{+} strength in these four N=28 nuclei as found in our (p,p') data is in general agreement with that obtained from (e,e')[34] and (γ,γ)[35]. For ^{51}V, however, where we observe a strong resonance centered at 10.15 MeV (Fig. 10), no M1 transitions at all are seen in (e,e')[36].

In a nucleus where the M1 transition proceeds only by a neutron excitation, such as in ^{90}Zr or ^{48}Ca, and assuming that there are no correlations in the ground state, the isospin of the excited state is the same as the isospin, T_o, of the ground state. However, in a nucleus with both

neutron and proton valence orbits, the particle and hole can couple to isospin t = 0 and t = 1, the latter then coupling to the core to produce states of isospin T_o and T_o+1. The first observations we have made of the T_o+1 component were in (p,p') measurements on the Ni isotopes.[37] The spectra in Fig. 12 may be characterized as having two components, one a broad component with much fine structure around 7-11 MeV, the other a sharp peak which moves to higher excitation energy as the mass of the target increases. The broad peak is identified mainly with the T = T_o component of the M1 resonance and the sharp peak as part of the T = T_o+1 component. In ^{60}Ni, there are other smaller peaks, presumably pieces of the T_o+1 component. This trend is even stronger in ^{58}Ti, where the two components are not well separated in energy. The energetics for ^{60}Ni are displayed in Fig. 14. If our isospin assignment is correct, the state at 11.85 MeV is a 1^+, T=3 state. Although above the neutron threshold, neutron emission from this state would be isospin forbidden. Emission of an ℓ=3 proton with 2.32 meV is allowed, but the Coulomb-centrifugal barrier ensures that the decay width is small. Since the level density of T=3 states near 12 MeV is not large, the spreading width of the 1^+, T=3 state is also small, and the state has a narrow total width. Similar arguments apply for the other Ni isotopes. Even in ^{64}Ni, where the T_o+1 level occurs at 15.62 MeV excitation energy, its observed width is limited by the experimental resolution of about 70 keV.

Finally, as a confirmation of our understanding of the structure in the Ni isotopes, it is interesting to return to the (p,n) reaction. The energetics of the ^{60}Ni(p,n) ^{60}Cu are also given in Fig. 14. We see that three 1^+ states are expected with isospins, 3, 2 and 1. the T=3 and T=2 states being analogues of the structures observed in (p,p'). Spectra from the (p,n) reaction carried out by a Kent State-MSU collaboration at IUCF on ^{58}Ni, ^{60}Ni, ^{62}Ni and ^{64}Ni are shown in Fig. 15. The expected components are seen, particularly the sharp T = T_o+1 component in the three lighter Cu isotopes. Isospin geometry strongly disfavors transitions to the T_o+1 states, particularly when T_o is large.

Stimulated by the striking (e,e') data[38] obtained at Darmstadt on Ca isotopes, we have studied the (p,p') reactions on the same targets. Spectra taken at 3° are shown in Fig. 16. In ^{40}Ca, the well known 1^+ state at 10.31 MeV is observed. However, an additional state at 12.03 MeV is also seen with an ℓ=0 angular distribution. While this angular distribution does not distinguish a 1^+ from a 0^+, the selective excitation at high bombarding energy suggests a spin-flip excitation. No 1^+ state was observed in (e,e') near 12.03 MeV. A $0^+ \rightarrow 1^+$ transition in ^{40}Ca must, of course, involve core excitations of both neutrons and protons. There could, therefore, be cancellation between the orbital and spin parts of the B(M1) amplitude. In ^{42}Ca, no strongly excited 1^+ transitions are observed, as can be seen in Fig. 16. This is in contrast with the (e,e') where a 1^+ state at

11.24 MeV was seen with a B(M1) value of $0.59 \pm 0.05\ \mu^2_N$. This is therefore about 16% of the strength of the single sharp state observed in ^{48}Ca. This state is indicated in Fig. 16. Its angular distribution is identical to that of the strong, definite 1^+ state in ^{48}Ca, but its relative cross section is down by a factor of 30, not 6. There are additional states with forward peaked angular distributions at 10.08, 10.24, and 11.40 MeV, each with strength comparable to or greater than the strength of the 10.24 MeV state. These are likely to be 1^+ states also. Again, one must appeal to an orbital contribution in (e,e') to explain the lack of detailed agreement. In ^{44}Ca(p,p') there are seven states whose forward peaked angular distributions imply 1^+. The cross sections for those various peaks are comparable to each other. Fragmentation of M1 strength was similarly found in ^{44}Ca(e,e').

The (p,p') spectrum for ^{48}Ca is a very dramatic one. Indeed, in no other target have we seen such an extreme concentration of ℓ=0, spin-flip strength. As shown in Fig. 17, this concentration allows a beautiful demonstration of the ℓ=0 selectivity at small angles. The analogous GT transition has already been discussed in connection with Fig. 7. Detailed investigation[39] of ^{48}Ca should be fruitful because of the simplicity of its shell-model wave function. Experimentally, the sharpness of the peak leaves little ambiguity in the background subtraction, so that the cross section can be obtained quite accurately. In addition to the strong

10.2 MeV state, eighteen additional 1^+ states were observed[34] in (e,e') between 7.7 and 12.7 MeV. These raise the total value of B(M1) from $3.7 \pm 0.3\ \mu_N^2$ for the single state, to $5.0\ \mu_N^2$. In the same interval of excitation energy, we see fteen, additional states. Seven of these are within 42 keV of an (e,e') state. The other states seem not to be correlated in energy. The angular distributions of most of our states have some forward peaking but possibly because of the presence of unresolved states of higher spin, none has a shape matching that of the strong state. Some of these angular distributions are given in Fig. 18; the 10.2 MeV data are included for comparison.

Microscopic distorted wave calculations have been carried out using the codes RESEDA and DWBA 70. The 10.2 MeV data and the computed differential cross sections are given in Fig. 19. The calculations used a closed $(f_{7/2})$ shell for the 0^+ ground state, a simple $(f_{5/2})(f_{7/2})^{-1}$ configuration for the 1^+ state at 10.2 MeV. The RESEDA calculation used phase shifts from the Paris potential[40], and the DWBA 70 calculations used the Love-Franey parameterization of the interaction. The ratio of experimental to theoretical cross section is 0.24 for the RESEDA calculation and 0.21 for the DWBA 70 calculation. The ratio in the latter case increases to 0.30 when a full f-p shell basis[41] is used to generate the wave functions.

As discussed above (equation 4), in ^{48}Ca, where the 1^+ excitation is almost entirely a neutron excitation, any

quenching should appear in (p,p'), (p,n) and (e,e') reactions in comparable proportions. Since only the sharp peak at 10.2 MeV is observed consistently in the different reactions, we will restrict our strength comparisons to this state.

A summary of the quenching in the ^{48}Ca(p,n) reaction was given in a recent paper by Osterfeld et al.[42] The calculations include results obtained with three different sets of wave functions: pure particle-hole, standard RPA, and RPA including the Δ isobar. These results are summarized in Table 2 together with values from the present and previous (p,p') measurements. The quenching of the B(M1) value for the 10.2 MeV 1^+ state excited by (e,e') is also given in this table. The absolute magnitude of the (p,p') cross section is generally overpredicted by a factor of 3 to 4, the exact value depending on the details of the wave functions used. The ratio of predicted to experimental cross section from our measurement is qualitatively consistent with the ratio observed in (p,n) and (e,e') reactions.

IV. Closing Thoughts

Seeing that all three reactions report significant quenching, it is of some interest to compare the properties of the three probes. The (p,n) reaction has the advantage of a sum rule (equation 2) that is almost model independent; only the β^+ strength must be computed, and in most nuclei Pauli blocking makes that strength a small correction to 3(N-Z). The (e,e') reaction depends for its theoretical

B(M1) on wave functions. Hopefully, in the case of ^{48}Ca that is not a serious problem, but we are not sure. In (p,p') the comparison is to a computed cross section that depends on wave functions, on the nucleon-nucleon interaction, and somewhat on the DWIA, i.e., on optical potentials.

Experimentally, (e,e') has difficulty with heavy nuclei. It is hard to find a bombarding energy high enough so that the radiative tail is small and yet low enough that M2 transitions are not enhanced over M1 transitions. In (p,p') (as compared to (p,n)) one cannot go quite to 0^o, but the energy resolution is much better and there are fewer T_z components in which the 1^+ strength resides. A comparison of Figs. 7 and 17 illustrates these two points quite well.

Even under such good experimental conditions as in Fig. 17, the interpretation of the (p,p') results in terms of quenching is sensitive to the interaction because both isoscalar and isovector spin-flip operators are involved in $0^+ \rightarrow 1^+$ transitions, unless the nucleus has N=Z. Recently, we have taken (p,p') data at 200 meV on some self-conjugate nuclei. In ^{28}Si, for example, we have found both T=1 and T=0, 1^+ states. A spectrum at 3^o is shown in Fig. 20. Using Wildenthal's s-d shell wave functions in the distorted waves calculations, we find quenching in both the pure isovector and the pure isoscalar channels. The ratio of experimental to theoretical cross section when summed over all the observed 1^+ states is 0.40 for T=1 states and 0.25 for T=0 states. Both numbers are in line with what we have come to

expect for quenching. For the T=0 states, the Δ resonance is not, of course, a possible explanation. If, in spite of the sensitivity to wave functions and interaction, the observed T=0 quenching is correct, it must come from configuration mixing. Would we then need the Δ for T=1 quenching? Perhaps further study of isoscalar spin-flip quenching will shed some light on the origin of isovector spin-flip quenching.

References

1. J.D. Anderson and C. Wong, Phys. Rev. Lett. 7, 250 (1961).
2. R.R. Doering, A. Galonsky, D.L. Patterson and G.F. Bertsch, Phys. Rev. Lett. 35, 1691 (1975).
3. K. Ikeda, S. Fujii and J.I. Fujita, Phys. Lett. 3, 271 (1963).
4. C.D. Goodman et al., IEEE Trans. Nucl. Sci. 26, 2248 (1979).
5. C.D. Goodman, J. Rapaport, D.E. Bainum and C.E. Brient, Nucl. Instr. and Meth. 151, 125 (1978).
6. A. Fazely et al., Phys. Rev. C25, (1982).
7. D.E. Bainum et al., Phys. Rev. Lett. 44, 1751 (1980).
8. C.D. Goodman et al., Phys. Rev. Lett. 44, 1755 (1980).
9. C. Gaarde, J.S. Larsen and J. Rapaport, Conference on Spin Excitations in Nuclei, Telluride, March 1982.
10. W.G. Love and M.A. Franey, Phys. Rev. C24, 1073 (1981).
11. T.N. Taddeucci et al., Phys. Rev. C 25, 1094 (1982).
12. C. Gaarde, et al., Nucl. Phys. A334, 248 (1980).
13. F. Petrovich, W.G. Love and R.J. McCarthy, Phys. Rev. C 21, 1718 (1980).
14. F. Osterfeld, Phys. Rev. C 26, 762 (1982).
15. G. Bertsch and O. Scholten, Phys. Rev. C 25, 804 (1982).

16. G. Bertsch and I. Hamamoto, Phys. Rev. C 26, 1323 (1982).

17. M. Ericson et al., Phys. Lett. 45B, 19 (1973); E. Oset and M. Rho, Phys. Rev. Lett. 42, 47 (1979); A. Bohr and B. Mottelson, Phys. Lett. 100B, 10 (1981); A. Harting et al., Phys. Lett. 104B, 261 (1981).

18. C.G. Cassapakis et al., Phys. Lett. 63B, 35 (1976).

19. C. Ellegard et al., Phys. Rev. Lett. 50, 1745 (1983).

20. B.D. Anderson et al., Phys. Rev. Lett. 45, 699 (1980).

21. L.W. Fagg, Rev. Mod. Phys. 47, 683 (1975).

22. D. Meuer et al., Nucl. Phys. A349, 309 (1980).

23. F.E. Cecil, G.T. Garvey and W.J. Braithwaite, Nucl. Phys. A232, 22 (1974).

24. N. Anantaraman et al., Phys. Rev. Lett. 46, 1318 (1981).

25. G.M. Crawley et al., Phys. Rev. C 26, 87 (1982).

26. A. Willis et al., Nucl. Phys. A 344, 137 (1980).

27. F.E. Bertrand et al., Phys. Lett. 103B, 326 (1981).

28. S.K. Nanda et al., Preprint.

29. J. Raynal and R. Schaeffer, CEN, Saclay report, unpublished (1970).

30. A. Willis, Ph.D. Thesis, University of Paris, unpublished (1968).

31. C. Djalali et al., Nucl. Phys. A388, 1 (1982).

32. G.F. Bertsch, Nucl. Phys. A354, 157 (1981).

33. B.C. Metsch and W. Knupfer, private communication.

34. G. Eulenberg et al., Phys. Lett. 116B, 113 (1982) and private communications from W. Steffen and A. Richter.

35. U.E.P. Berg et al., Phys. Lett. 103B, 301 (1981) and Nucl. Phys. A 398, 397 (1983).

36. D. Bender et al., Nucl. Phys. A398, 408 (1983).

37. N. Marty et al., Nucl. Phys. A396, 145c (1983).

38. W. Steffen et al., Phys. Lett. 95B, 23 (1980) and private communication.

39. G.M. Crawley et al., Phys. Lett. 127B, 322 (1983).

40. M. Lacombe et al., Phys. Rev. C 21, 861 (1980).

41. J.B. McGrory and B.H. Wildenthal, Phys. Lett. 103B, 173 (1981).

42. F. Osterfeld et al., Phys. Rev. Lett. 49, 11 (1982).

Figure Captions

Fig. 1. Neutron time-of-flight spectrum at 0^{o} for $^{90}Zr(p,n)$ at E_p = 35 MeV. The Fermi (F) and Gamow-Teller (GT) peaks are indicated.

Fig. 2. Neutron spectra at 0.2^{o} for $^{90}Zr(p,n)$ at E_p = 80, 120, and 160 MeV. The Fermi (F) and Gamow-Teller (GT) peaks are indicated on the 120-MeV spectrum. The 160-MeV spectrum is a time, not energy, spectrum.

Fig. 3. Neutron energy spectra at various angles for $^{90}Zr(p,n)$ at E_p = 120 MeV. The Fermi (F) and Gamow-Teller (GT) peaks are indicated on the 0.1^{o} spectrum.

Fig. 4. Gamow-Teller strength observed in (p,n) reactions as a percentage of the sum rule limit $3(N-Z)+S_{\beta+}$. Values of $S_{\beta+}$ have been estimated. See Ref. 9.

Fig. 5. Neutron spectrum from proton collisions with ^{12}C and ^{27}Al at 0^{o} and 800 MeV incident energy. The peak occurs 300 MeV below the bombarding energy. See Ref. 18.

Fig. 6. Relationships between (p,n), (p,p') and electromagnetic interactions for exciting 1^{+} states.

Fig. 7. Neutron spectrum at 0^{o} from p + ^{48}Ca at 160 MeV. The peak at 16.8 MeV represents a 1^{+}, T=4 state. The other 1^{+} states have T=3. See Ref. 20.

Fig. 7a. Spectra of 200-MeV protons inelastically scattered from ^{90}Zr, ^{92}Zr, ^{94}Zr and ^{96}Zr at 4^{o}. The arrows indicate the centroids of the M1 resonance.

Fig. 8. Angular distributions for the M1 state in ^{90}Zr, ^{92}Zr, ^{94}Zr and ^{96}Zr observed in (p,p') at 200 MeV. The solid curves are DWBA 70 calculations and the dashed curve is a RESEDA calculation. All calculations are normalized to the data at forward angles. The dotted-dashed curve is from a $^{90}Zr(p,n)$ measurement at 200 MeV.

Fig. 9. Spectra of 200-MeV protons inelastically scattered from ^{92}Mo, ^{94}Mo, ^{96}Mo, ^{98}Mo and ^{100}Mo at 4^{o}.

Fig. 10. Spectra of 200-MeV protons inelastically scattered from ^{51}V at 3^{o} & 8^{o}. At 3^{o} the overlap of two spectra taken with different magnetic fields is shown.

Fig. 11. Spectra of 200-MeV protons inelastically scattered from ^{48}Ca, ^{50}Ti, ^{52}Cr, and ^{54}Fe at 3^{o}.

Fig. 12. Spectra of 200-MeV protons inelastically scattered from ^{58}Ni, ^{60}Ni, ^{62}Ni, and ^{64}Ni at 4^{o}.

Fig. 13. Angular distributions for some representative 1^{+} states excited in $^{50}Ti(p,p')$ at 200 MeV. See Fig. 11. At the top is the angular distribution for the sum of all the 1^{+} states observed and a theoretical curve (see Ref. 33) scaled by the factor 0.39 to fit the data.

Fig. 14. Energetics of 1^+ states excited in ^{60}Ni by (p,p') and in ^{60}Cu by (p,n). Cross hatching indicates a broad state. Decay energies for proton and neutron emission from the sharp T=3 state at 11.85 MeV in ^{60}Ni are also shown.

Fig. 15. Neutron energy spectra from (p,n) reactions at 0^o on ^{58}Ni, ^{60}Ni, ^{62}Ni and ^{64}Ni at 134 MeV.

Fig. 16. Spectra of 200-MeV protons inelastically scattered from ^{40}Ca, ^{42}Ca, ^{44}Ca and ^{48}Ca at 3^o.

Fig. 17. Spectra of protons inelastically scattered from ^{48}Ca at angles from 2^o to 12^o. The uppermost spectrum has been scaled to show the weakly excited states.

Fig. 18. Angular distributions of some of the weakly excited states (see top Fig. 17) in $^{48}Ca(p,p')$. The strong state at 10.2 MeV is included for comparison.

Fig. 19. Angular distribution for $^{48}Ca(p,p')$ to the 10.2 MeV state. The points are the measured values and the curves are from calculations described in the text.

Fig. 20. Spectrum of protons inelastically scattered from ^{28}Si through 3^o.

TABLE 1 : Summary of the results obtained in the 200 MeV (p,p') excitation of M1 resonances.

Nucleus	E_x (MeV) T_0	Γ (MeV) FWHM	E_x (MeV) T_0+1	Q
^{51}V	10.15 ± 0.15	1.35 ± 0.1	13.08	
^{58}Ni	8.5 ± 0.1 [a]		10.65	0.23 ± 0.03
			11.36 [b]	
^{60}Ni	8.9 ± 0.1 [a]		11.85	
			12.58 [b]	
^{62}Ni	8.8 ± 0.1 [a]		14.03	
^{68}Zn	9.6 ± 0.1	1.0 ± 0.1		
	8.6 ± 0.1	0.9 ± 0.2		
^{90}Zr	8.9 ± 0.2	1.5 ± 0.2		0.26 ± 0.03
^{92}Zr	8.8 ± 0.2	1.4 ± 0.2		
^{94}Zr	8.7 ± 0.2	1.4 ± 0.2		
^{96}Zr	8.6 ± 0.2	1.2 ± 0.2		
^{92}Mo	9.0 ± 0.1	1.1 ± 0.1		0.34 ± 0.05
	7.95 ± 0.1	0.70 ± 0.05		
^{94}Mo	8.6 ± 0.15	2.35 ± 0.15		
^{96}Mo	8.4 ± 0.15	2.3 ± 0.15		
^{98}Mo	8.5 ± 0.15	2.2 ± 0.2		
^{100}Mo	8.5 ± 0.15	2.8 ± 0.2		
^{120}Sn	8.4 ± 0.15			0.27 ± 0.05
^{124}Sn	8.7 ± 0.2			
^{140}Ce	8.6 ± 0.2			0.25 ± 0.07

Q is the attenuation factor defined in the text

a) Centroid energy

b) Centroid energy when high energy structures are included

TABLE 2. Comparison of experimental cross sections with predictions for the 10.2 MeV 1^+ state of ^{48}Ca and the analogous 1^+ state in ^{48}Sc.

Reaction	Beam Energy	Wave Function	Reaction Code	$\frac{\sigma\ (exp)}{\sigma\ (theory)}$
(p,p')	201 MeV	p-h	RESEDA	0.24
	201 MeV	p-h	DWBA70	0.21
	201 MeV	full f-p[a]	DWBA70	0.30
(p,n)	160 MeV	p-h	FROST-MARS	0.27
		RPA[b]	FROST-MARS	0.37
		RPA+Δ[b]	FROST-MARS	0.56
				$\frac{B(M1)\ exp}{B(M1)\ theory}$
(e,e')	30-50 MeV	p-h		0.31
		full f-p[a]		0.43

[a]Ref. 41

[b]Ref. 42

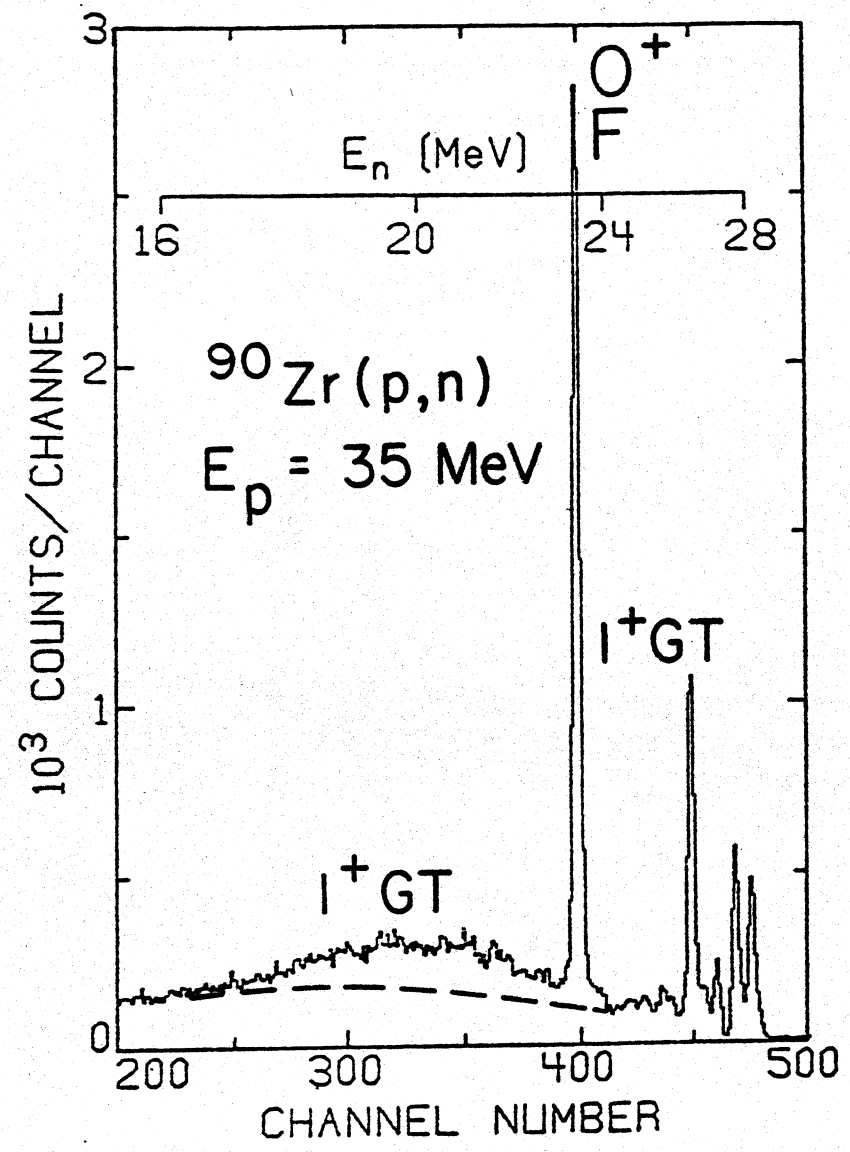
3
2
1
0
10^3 COUNTS/CHANNEL
E_n (MeV)
16
20
24
28
O^+
F
$^{90}Zr(p,n)$
E_p = 35 MeV
1^+GT
1^+GT
200
300
400
500
CHANNEL NUMBER

Fig. 1

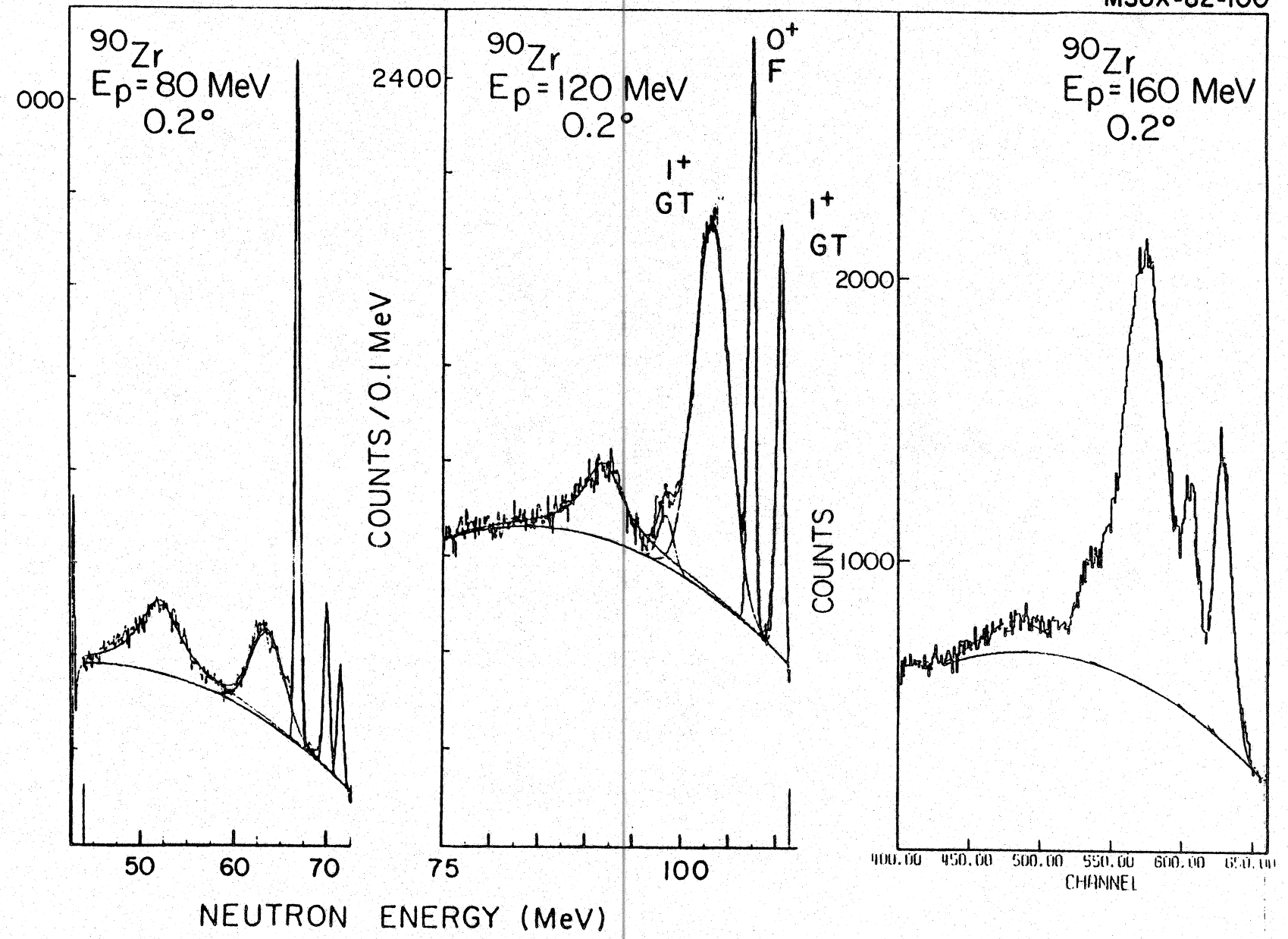
000
^{90}Zr
E_p=80 MeV
0.2°
2400
^{90}Zr
E_p=120 MeV
0.2°
0^+
F
1^+
GT
^{90}Zr
E_p=160 MeV
0.2°
1^+
GT
2000
1000
COUNTS
COUNTS/0.1 MeV
50
60
70
75
100
NEUTRON ENERGY (MeV)
400.00
450.00
500.00
550.00
600.00
CHANNEL

Fig. 2

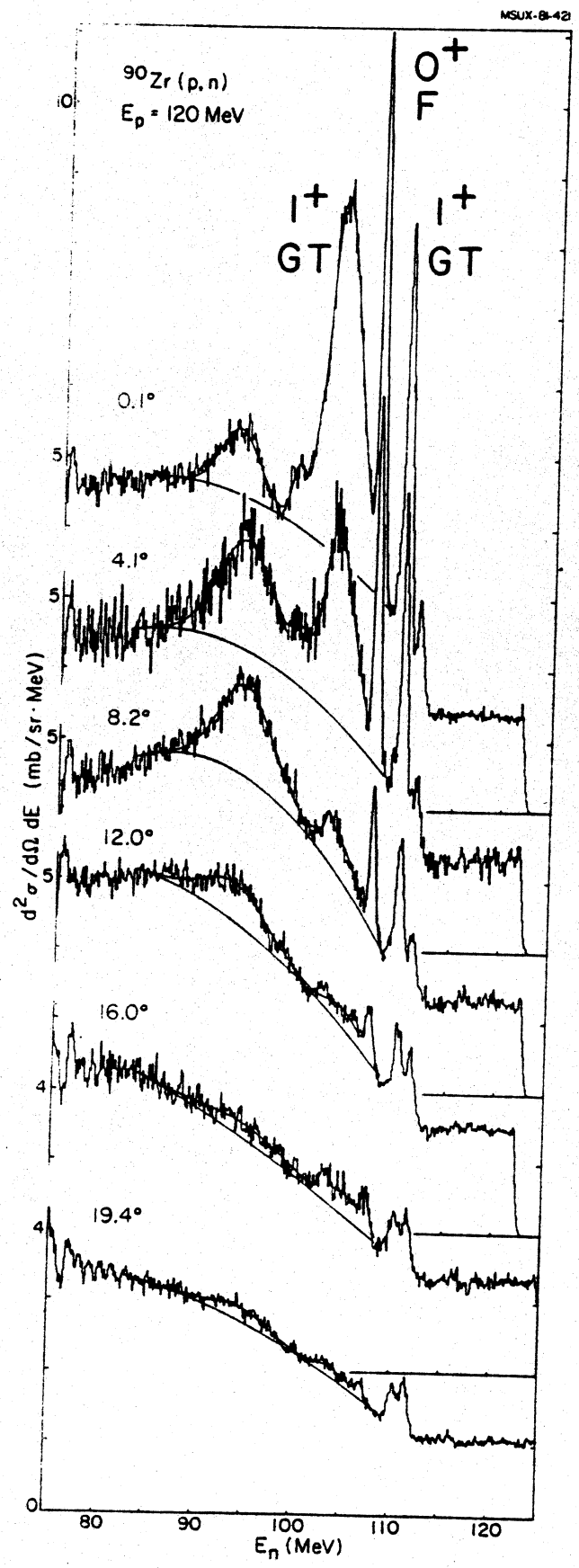
MSUX-81-42
^{90}Zr (p, n)
E_p = 120 MeV
0^+ F
1^+ GT
1^+ GT
0.1°
4.1°
8.2°
12.0°
16.0°
19.4°
$d^2\sigma/d\Omega\, dE$ (mb/sr·MeV)
E_n (MeV)
80
90
100
110
120

Fig. 3

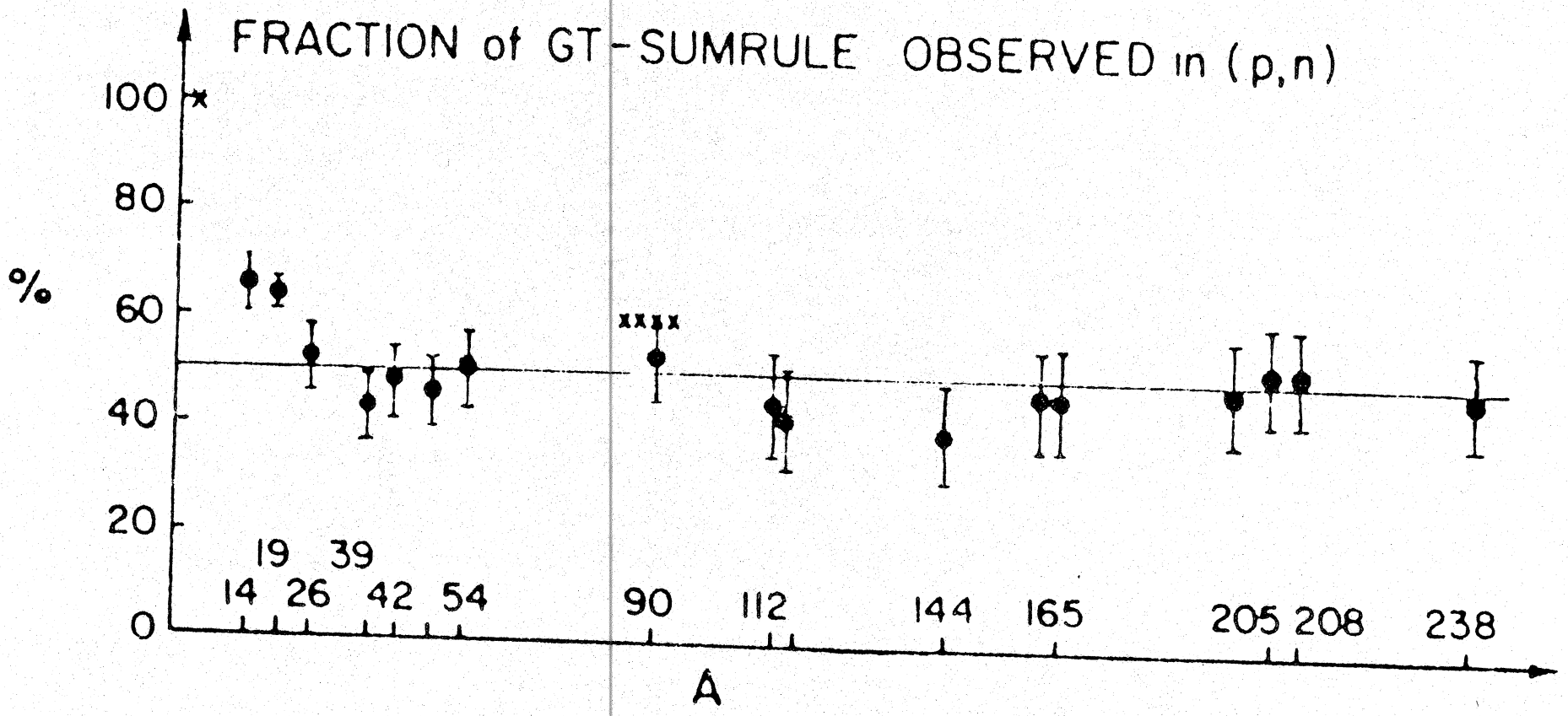
FRACTION of GT-SUMRULE OBSERVED in (p,n)
100
80
60
40
20
0
%
19
39
14
26
42
54
90
112
144
165
205
208
238
A

Fig. 4

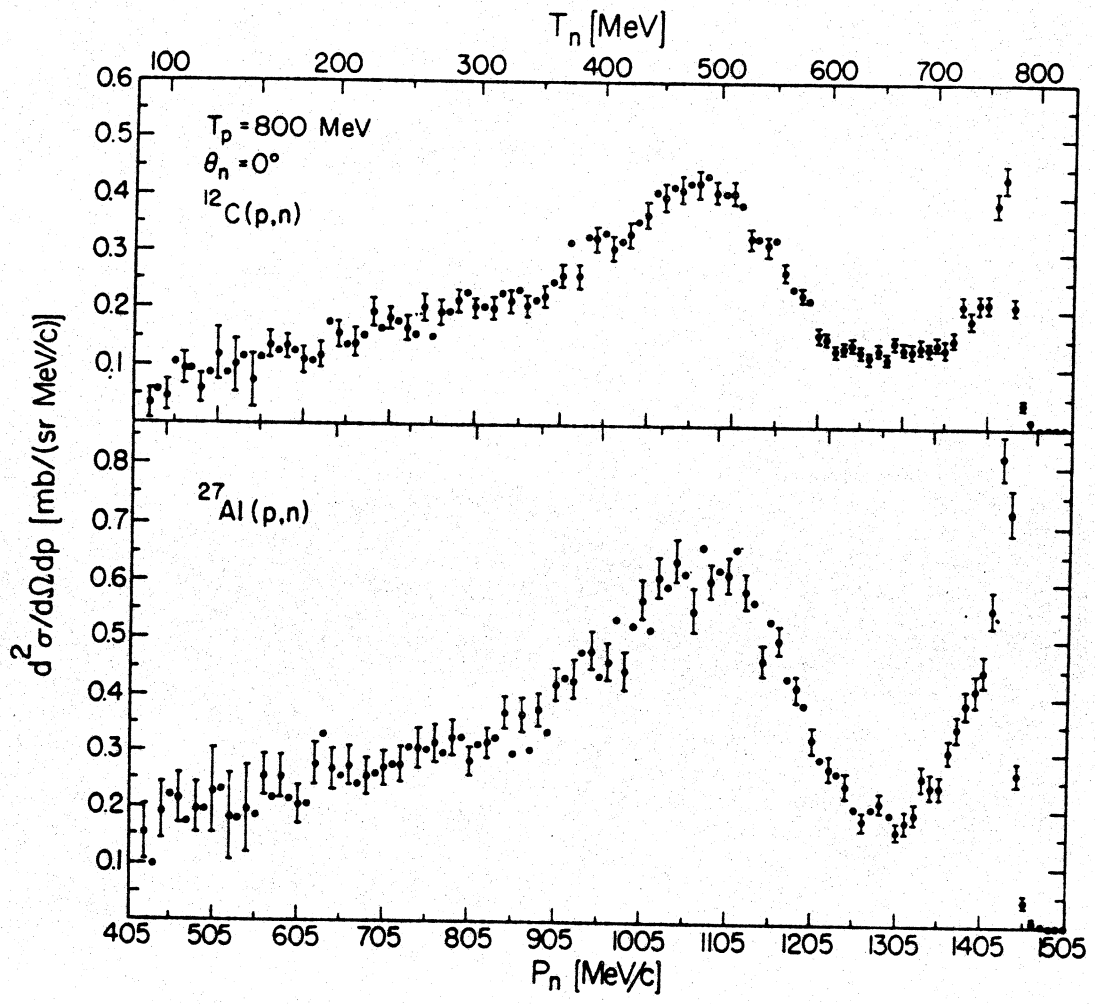
T_n [MeV]
100
200
300
400
500
600
700
800
T_p = 800 MeV
θ_n = 0°
^{12}C(p,n)
^{27}Al (p,n)
$d^2\sigma/d\Omega dp$ [mb/(sr MeV/c)]
0.1
0.2
0.3
0.4
0.5
0.6
0.7
0.8
405
505
605
705
805
905
1005
1105
1205
1305
1405
1505
P_n [MeV/c]

Fig. 5

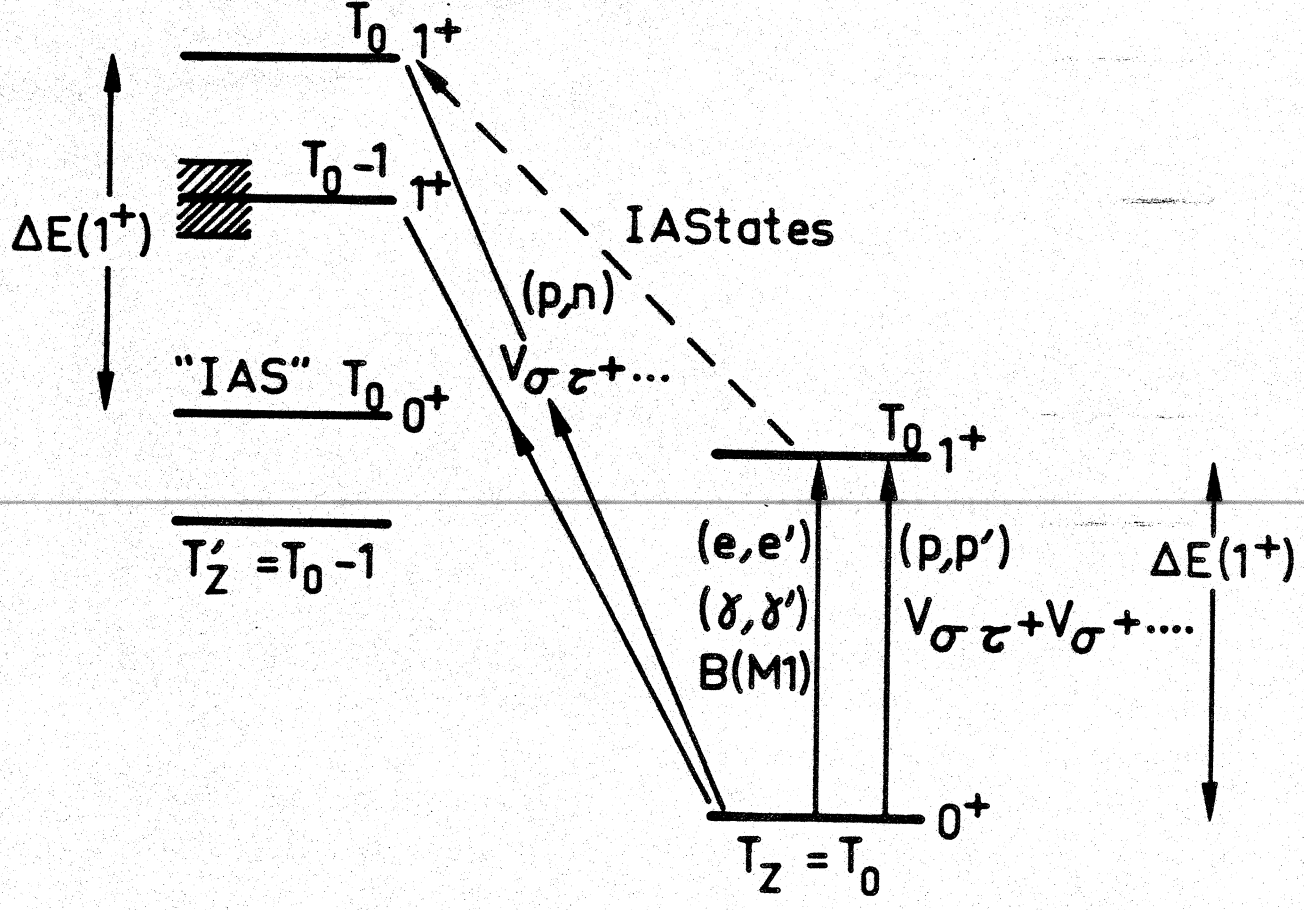
T_0 1^+
T_0-1 1^+
$\Delta E(1^+)$
IAStates
(p,n)
$V_{\sigma\tau}+\ldots$
"IAS" T_0 0^+
T_0 1^+
$T_z' = T_0-1$
(e,e')
(γ,γ')
B(M1)
(p,p')
$V_{\sigma\tau}+V_{\sigma}+\ldots$
$\Delta E(1^+)$
0^+
$T_z = T_0$

Fig. 6

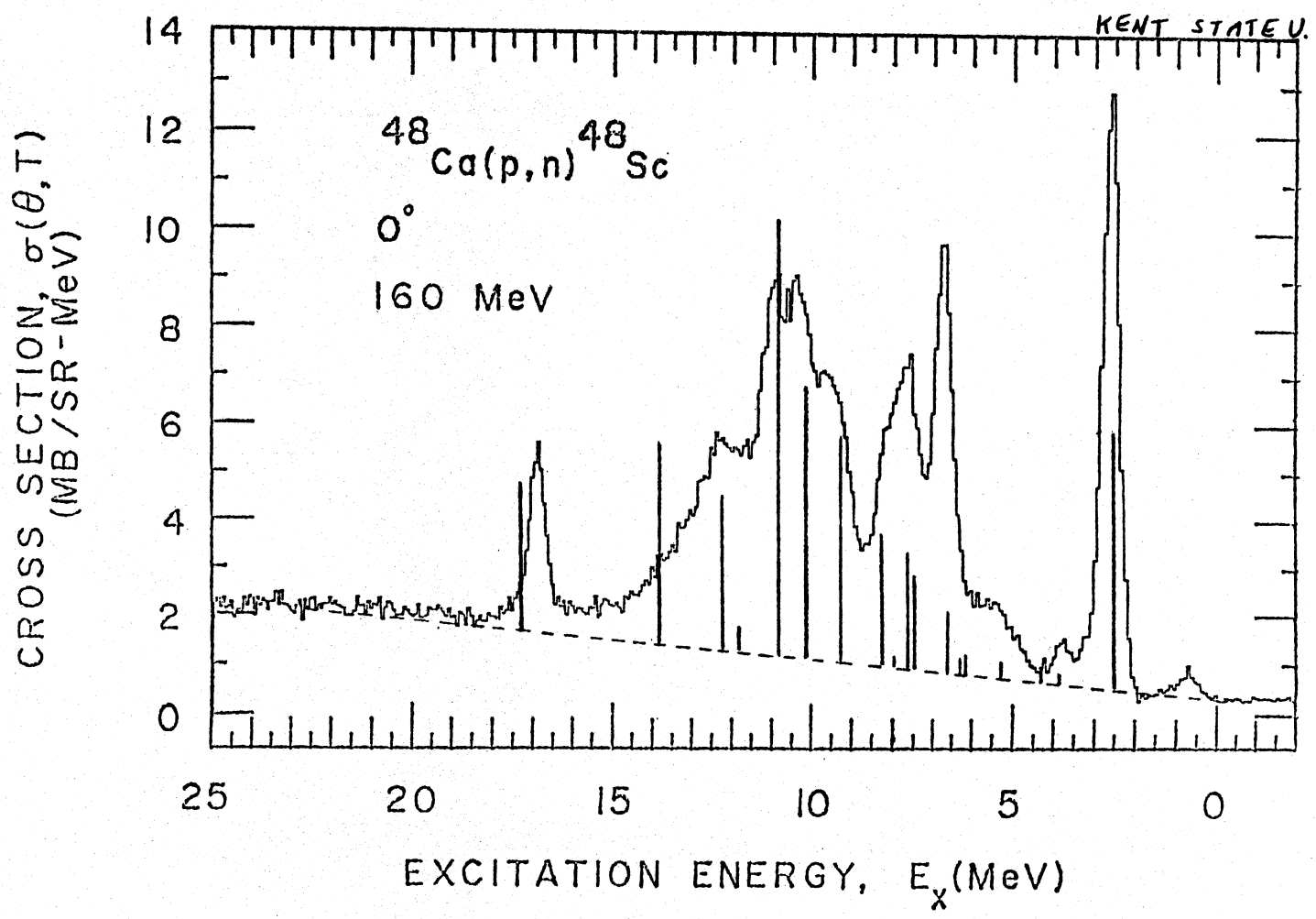
KENT STATE U.
$^{48}Ca(p,n)^{48}Sc$
0°
160 MeV
CROSS SECTION, $\sigma(\theta,T)$ (MB/SR-MeV)
14
12
10
8
6
4
2
0
25
20
15
10
5
0
EXCITATION ENERGY, E_x(MeV)

Fig. 7

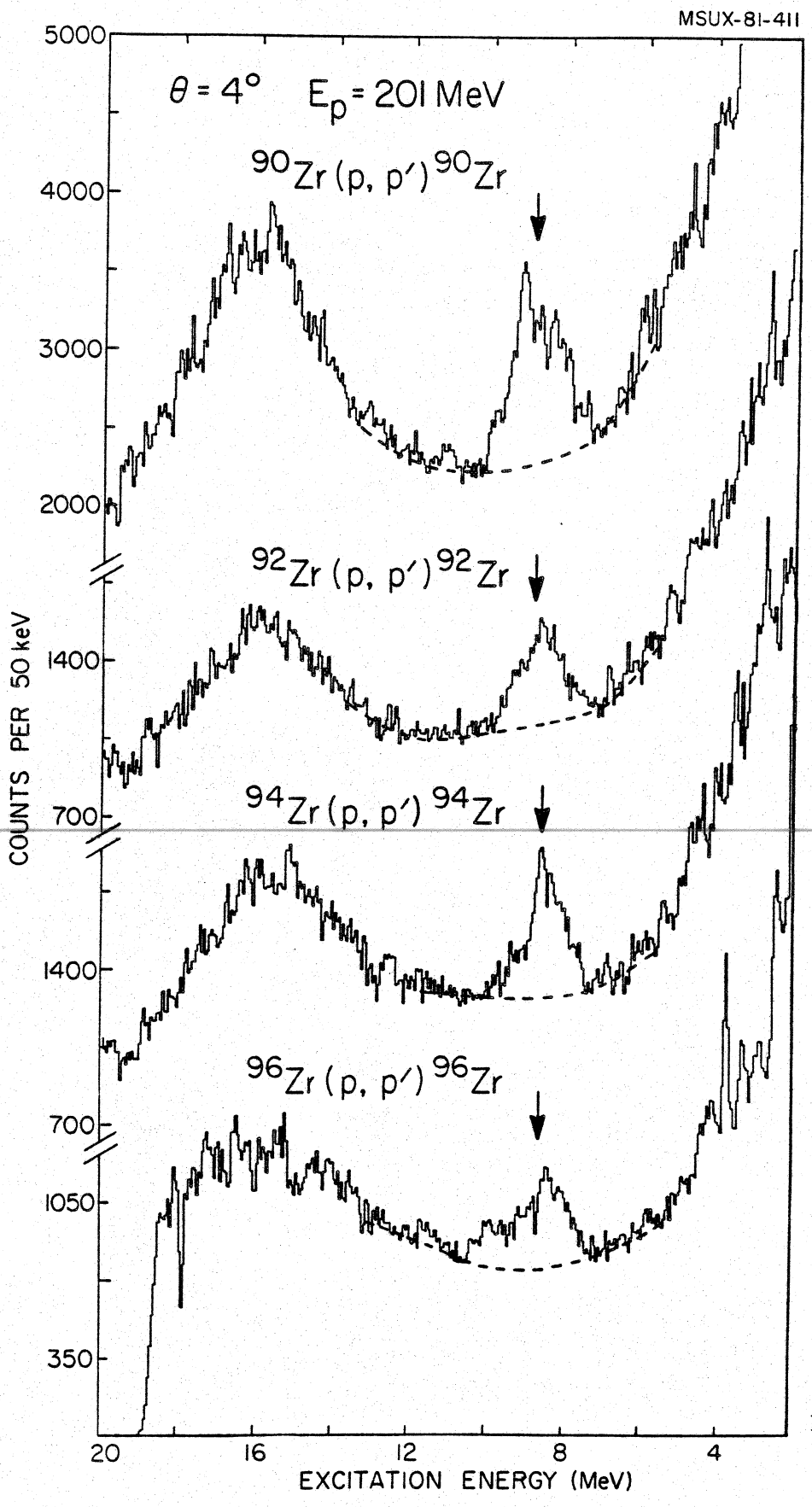
MSUX-81-411
θ = 4°
E_p = 201 MeV
90Zr (p, p′) 90Zr
92Zr (p, p′) 92Zr
94Zr (p, p′) 94Zr
96Zr (p, p′) 96Zr
COUNTS PER 50 keV
EXCITATION ENERGY (MeV)
5000
4000
3000
2000
1400
700
1400
700
1050
350
20
16
12
8
4

Fig. 7 a

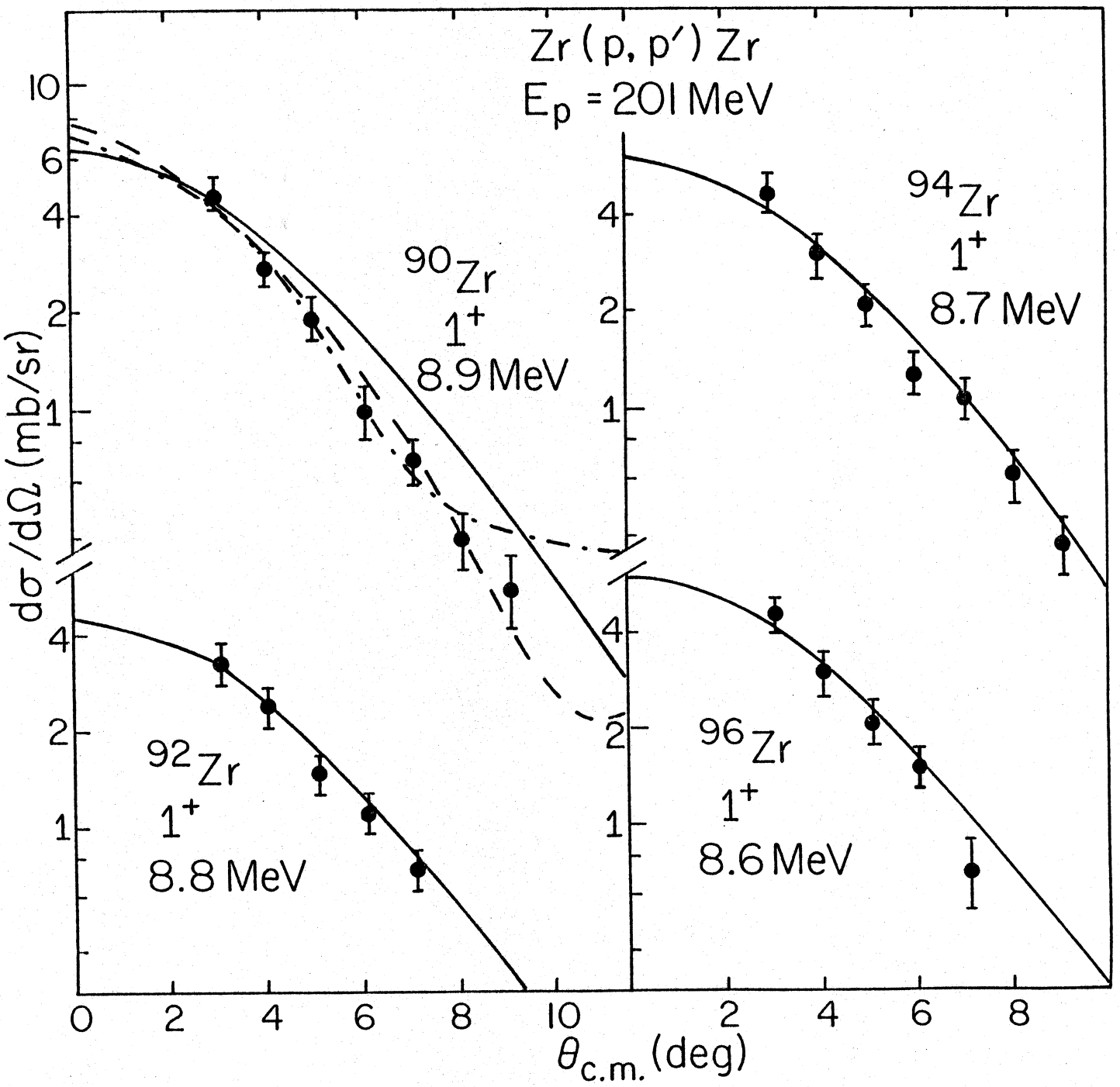
Zr (p, p′) Zr
Ep = 201 MeV
90Zr
1+
8.9 MeV
94Zr
1+
8.7 MeV
92Zr
1+
8.8 MeV
96Zr
1+
8.6 MeV
dσ/dΩ (mb/sr)
θc.m. (deg)

Fig. 8

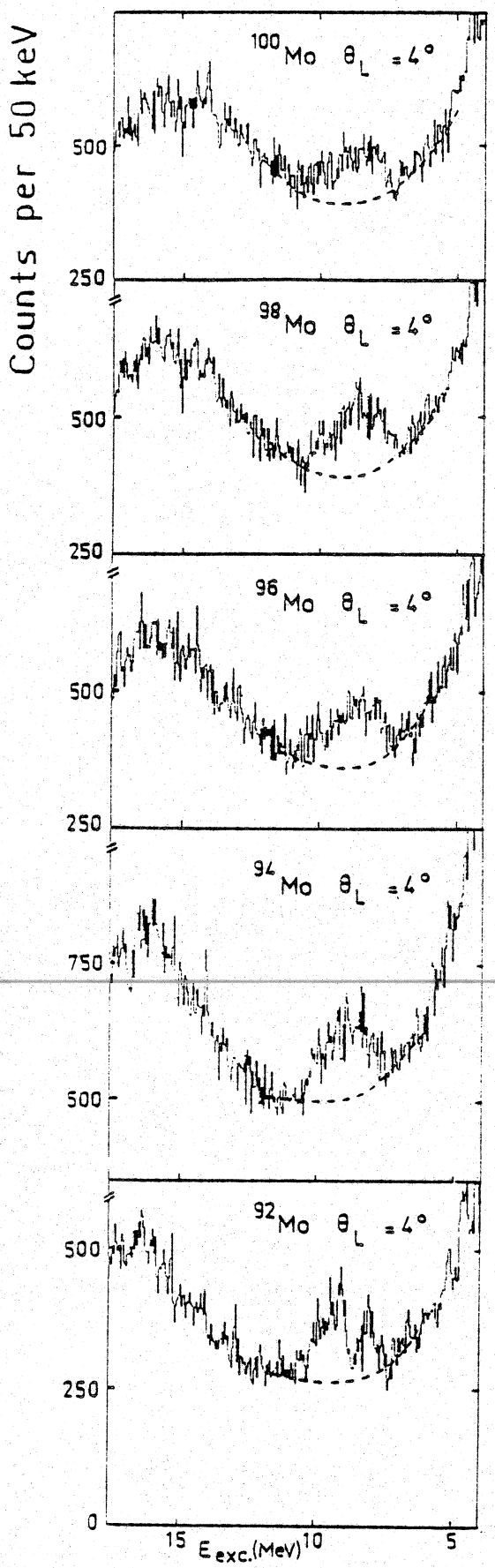
Counts per 50 keV
^{100}Mo θ_L = 4°
^{98}Mo θ_L = 4°
^{96}Mo θ_L = 4°
^{94}Mo θ_L = 4°
^{92}Mo θ_L = 4°
500
250
500
250
500
250
750
500
500
250
0
15
$E_{exc.}$(MeV)
10
5

Fig. 9

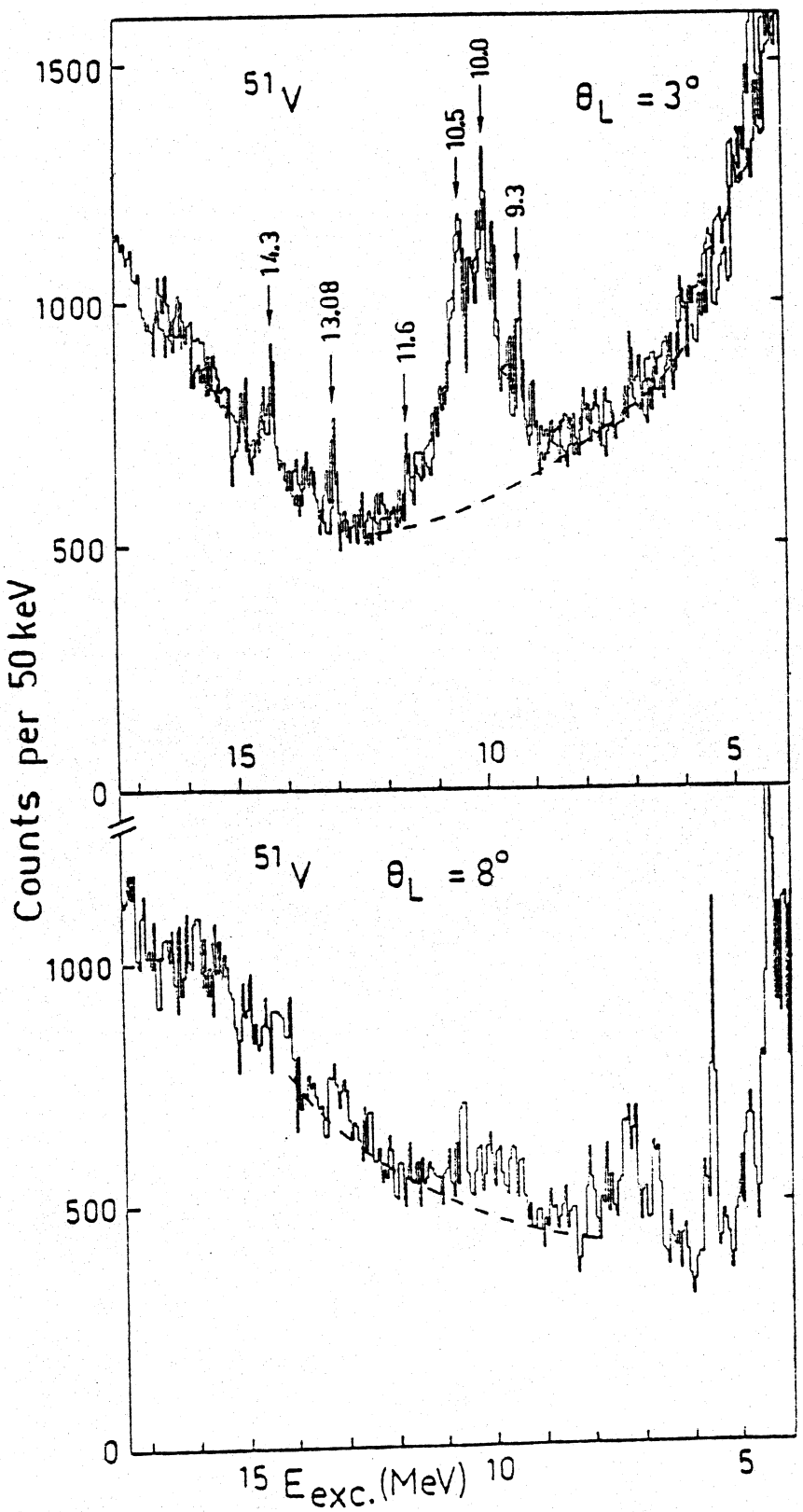
1500
1000
500
0
^{51}V
$\theta_L = 3°$
14.3
13.08
11.6
10.5
10.0
9.3
15
10
5
^{51}V
$\theta_L = 8°$
1000
500
0
Counts per 50 keV
15 $E_{exc.}$(MeV) 10
5

Fig. 10

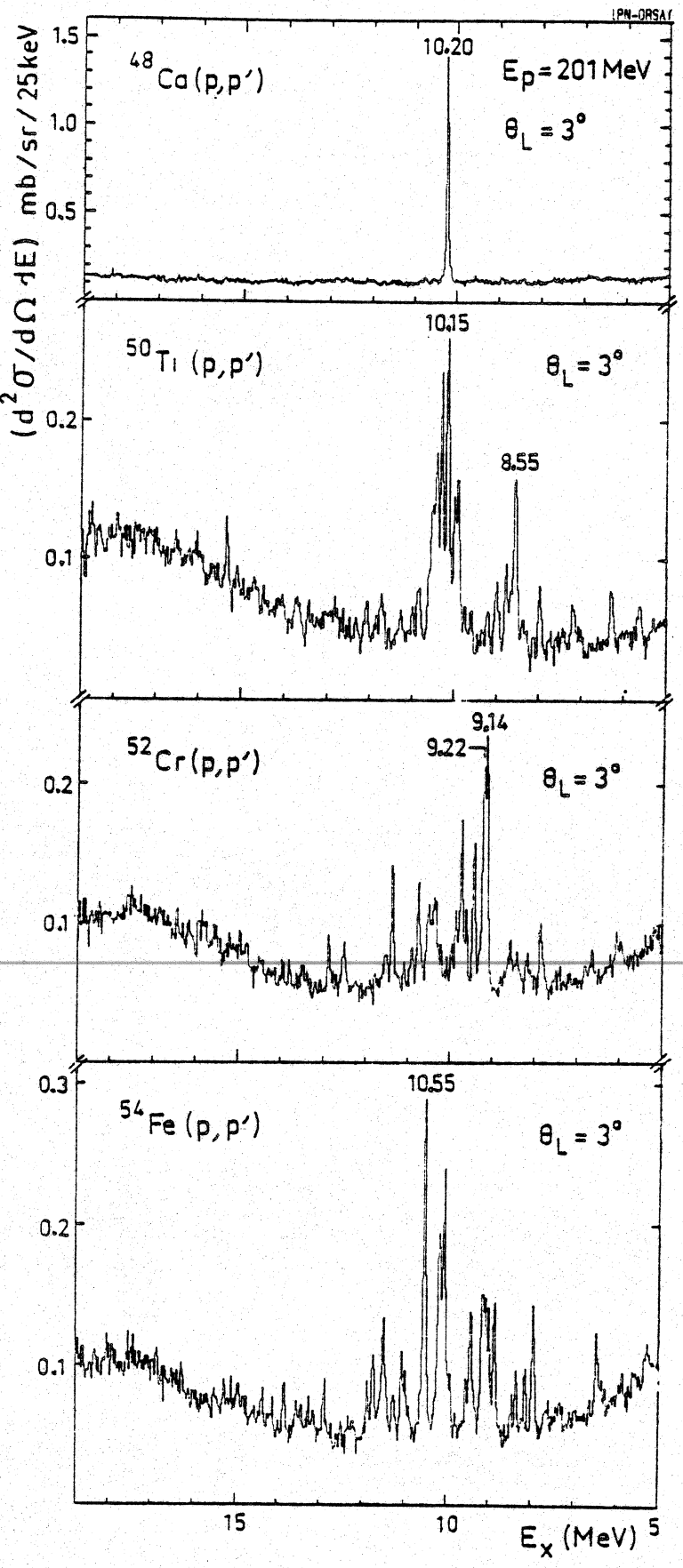
IPN-ORSAY
^{48}Ca(p,p')
10.20
E_p = 201 MeV
θ_L = 3°
^{50}Ti (p,p')
10.15
8.55
θ_L = 3°
^{52}Cr(p,p')
9.14
9.22
θ_L = 3°
^{54}Fe (p,p')
10.55
θ_L = 3°
$(d^2\sigma/d\Omega\,dE)$ mb/sr/25keV
1.5
1.0
0.5
0.2
0.1
0.3
15
10
5
E_x (MeV)

Fig. 11

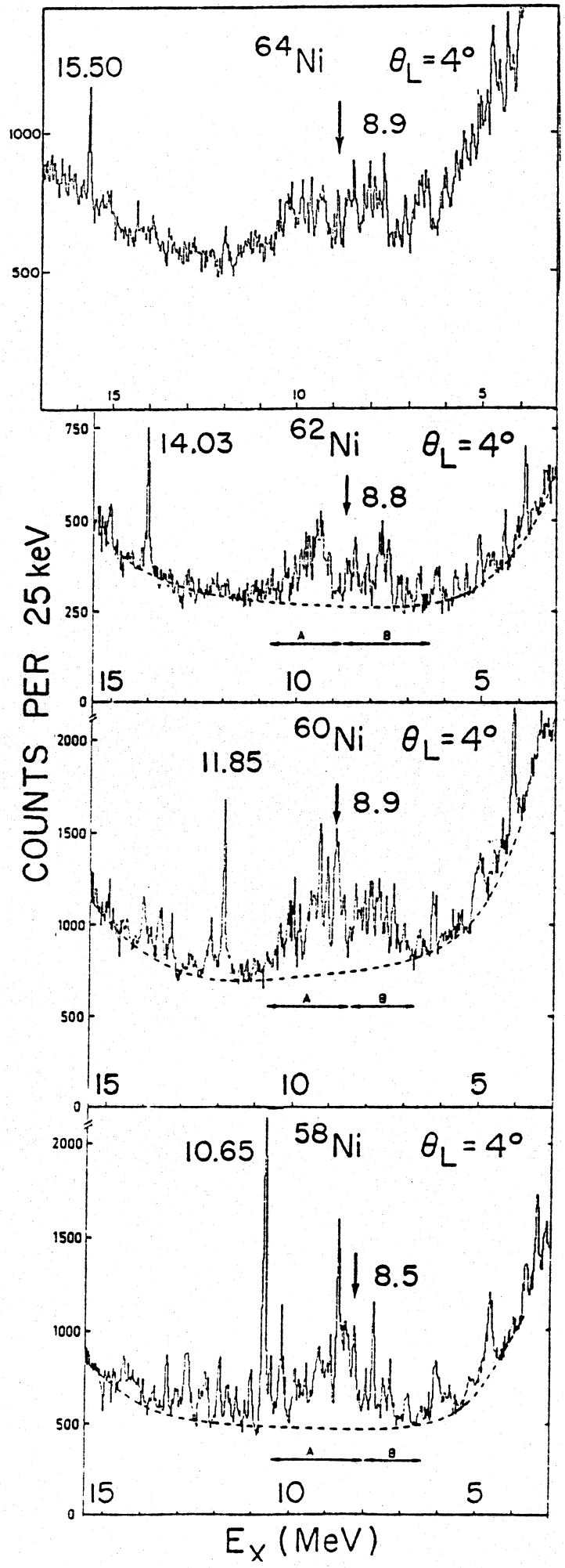
15.50
64Ni
θL=4°
8.9
1000
500
15
10
5
750
14.03
62Ni
θL=4°
8.8
500
250
A
B
15
10
5
0
2000
11.85
60Ni
θL=4°
8.9
1500
1000
500
15
10
5
0
2000
10.65
58Ni
θL=4°
8.5
1500
1000
500
15
10
5
0
COUNTS PER 25 keV
Ex (MeV)

Fig. 12

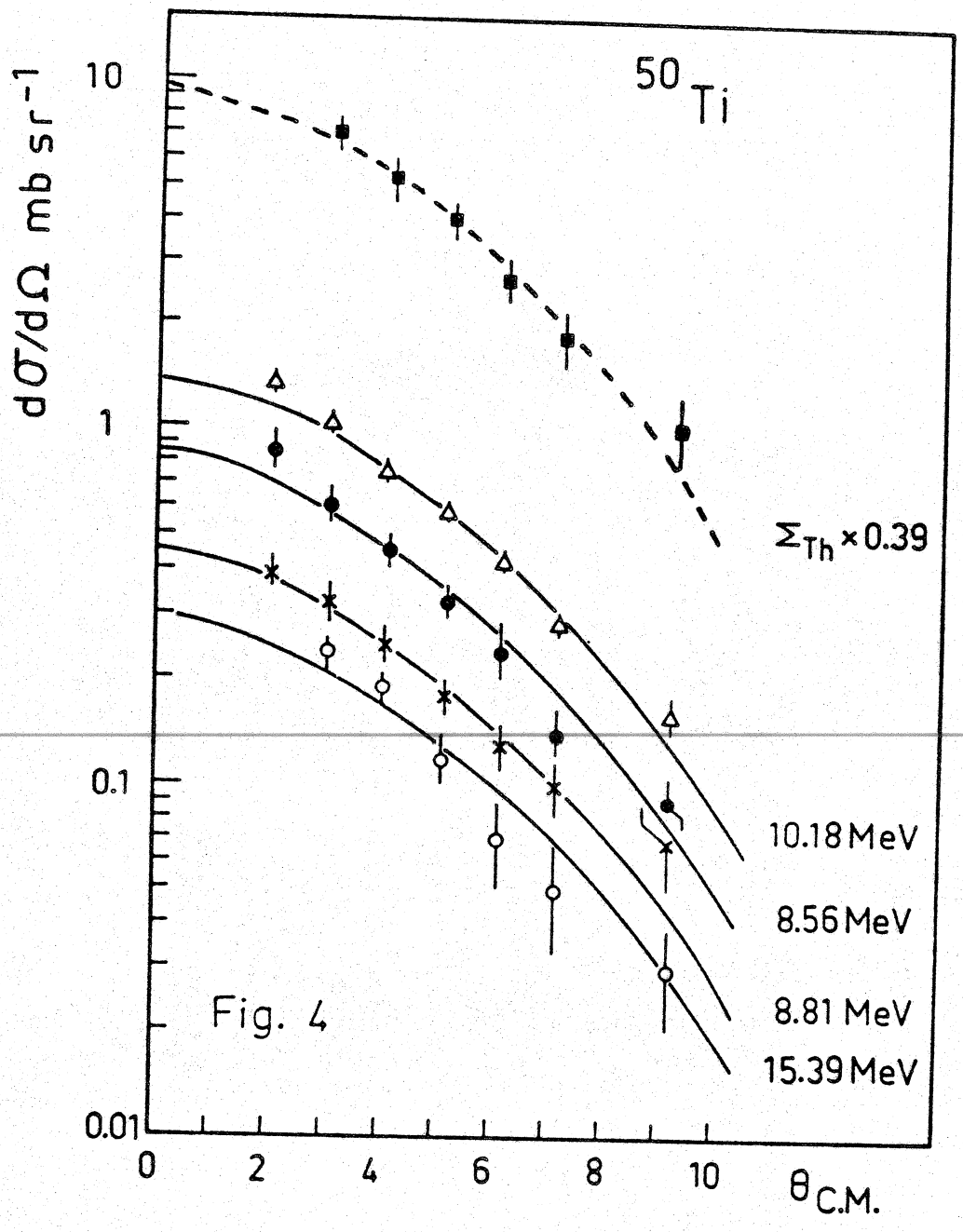
50 Ti
dσ/dΩ mb sr⁻¹
10
1
0.1
0.01
0
2
4
6
8
10
θ C.M.
Σ Th × 0.39
10.18 MeV
8.56 MeV
8.81 MeV
15.39 MeV
Fig. 4

Fig. 13

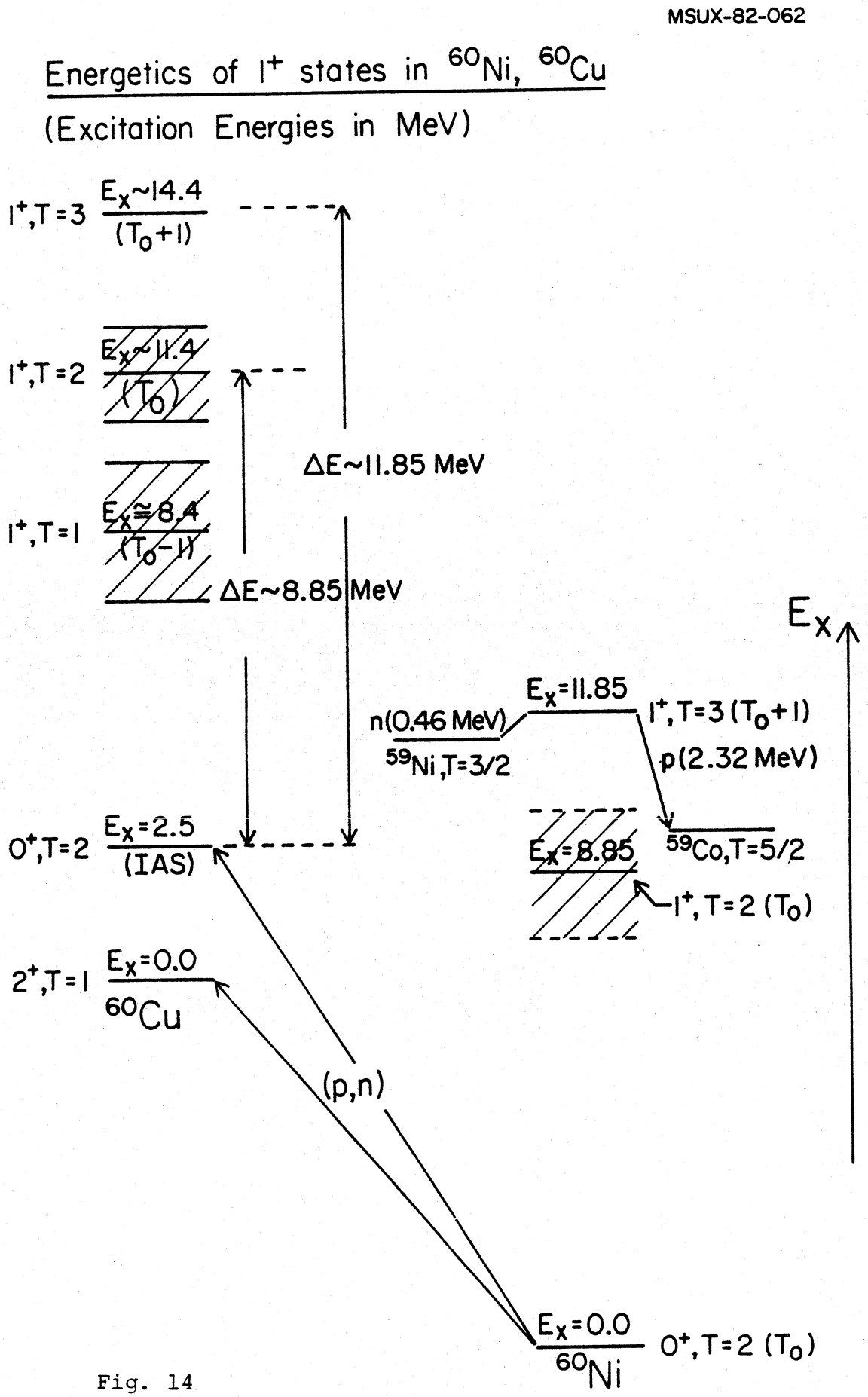
Energetics of 1^+ states in ^{60}Ni, ^{60}Cu
(Excitation Energies in MeV)
$1^+,T=3$ $E_x\sim14.4$ (T_0+1)
$1^+,T=2$ $E_x\sim11.4$ (T_0)
$1^+,T=1$ $E_x\cong8.4$ (T_0-1)
$\Delta E\sim11.85$ MeV
$\Delta E\sim8.85$ MeV
E_x
$E_x=11.85$
n(0.46 MeV)
$^{59}Ni,T=3/2$
$1^+,T=3$ (T_0+1)
p(2.32 MeV)
$E_x=8.85$
$^{59}Co,T=5/2$
$1^+,T=2$ (T_0)
$0^+,T=2$ $E_x=2.5$ (IAS)
$2^+,T=1$ $E_x=0.0$ ^{60}Cu
(p,n)
$E_x=0.0$ ^{60}Ni $0^+,T=2$ (T_0)

Fig. 14

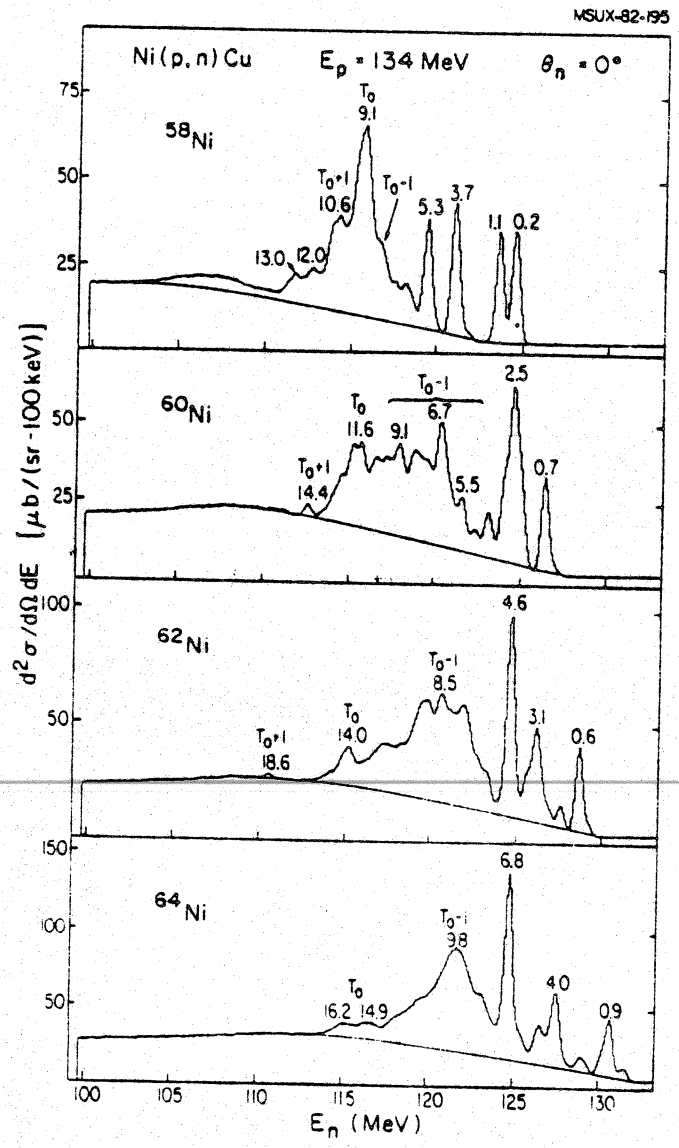
MSUX-82-195
Ni(p,n)Cu
E_p = 134 MeV
θ_n = 0°
^{58}Ni
T_0 9.1
T_0+1 10.6
T_0-1
5.3
3.7
1.1
0.2
13.0
12.0
^{60}Ni
T_0-1 6.7
T_0 11.6
9.1
T_0+1 14.4
2.5
0.7
5.5
^{62}Ni
4.6
T_0-1 8.5
T_0 14.0
T_0+1 18.6
3.1
0.6
^{64}Ni
6.8
T_0-1 9.8
T_0 16.2 14.9
4.0
0.9
$d^2\sigma/d\Omega dE$ [μb/(sr·100keV)]
E_n (MeV)

Fig. 15

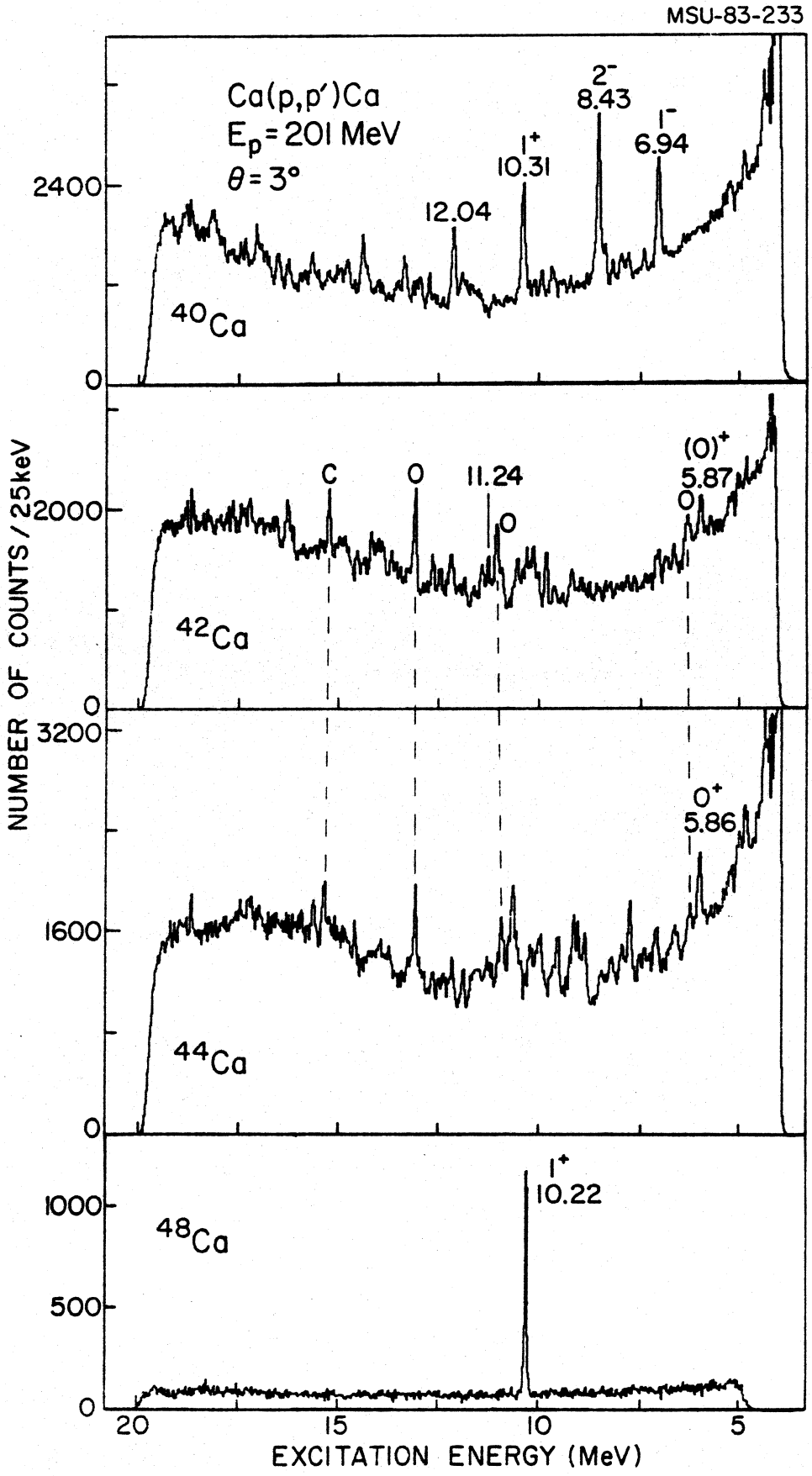
MSU-83-233
Ca(p,p')Ca
E_p = 201 MeV
θ = 3°
2⁻ 8.43
1⁻ 6.94
1⁺ 10.31
12.04
^{40}Ca
C
O
11.24
O
(0)⁺ 5.87
O
^{42}Ca
0⁺ 5.86
^{44}Ca
1⁺ 10.22
^{48}Ca
NUMBER OF COUNTS / 25keV
EXCITATION ENERGY (MeV)

Fig. 16

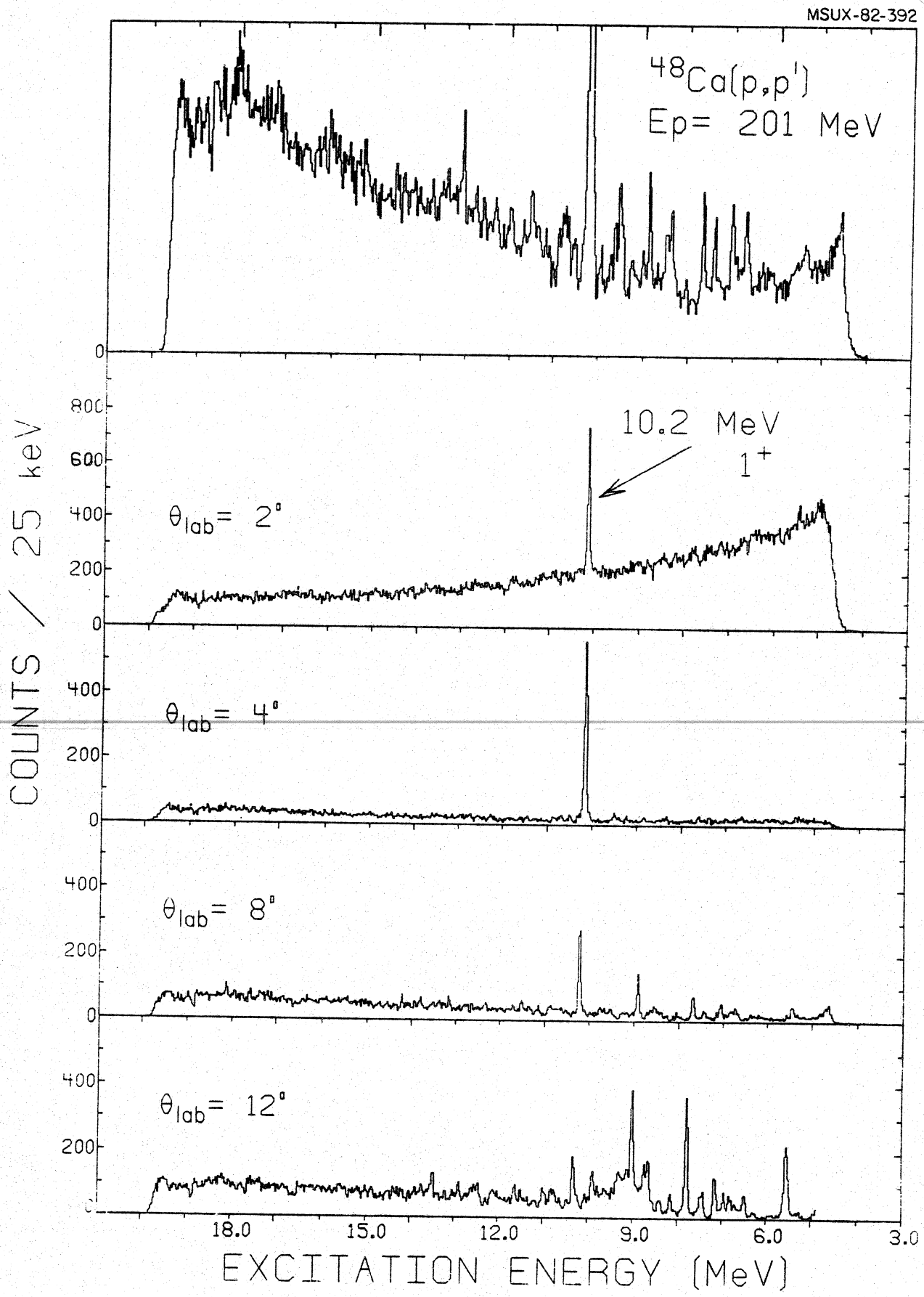
MSUX-82-392
^{48}Ca(p,p')
Ep= 201 MeV
10.2 MeV
1+
θlab= 2°
θlab= 4°
θlab= 8°
θlab= 12°
COUNTS / 25 keV
EXCITATION ENERGY (MeV)
18.0
15.0
12.0
9.0
6.0
3.0

Fig. 17

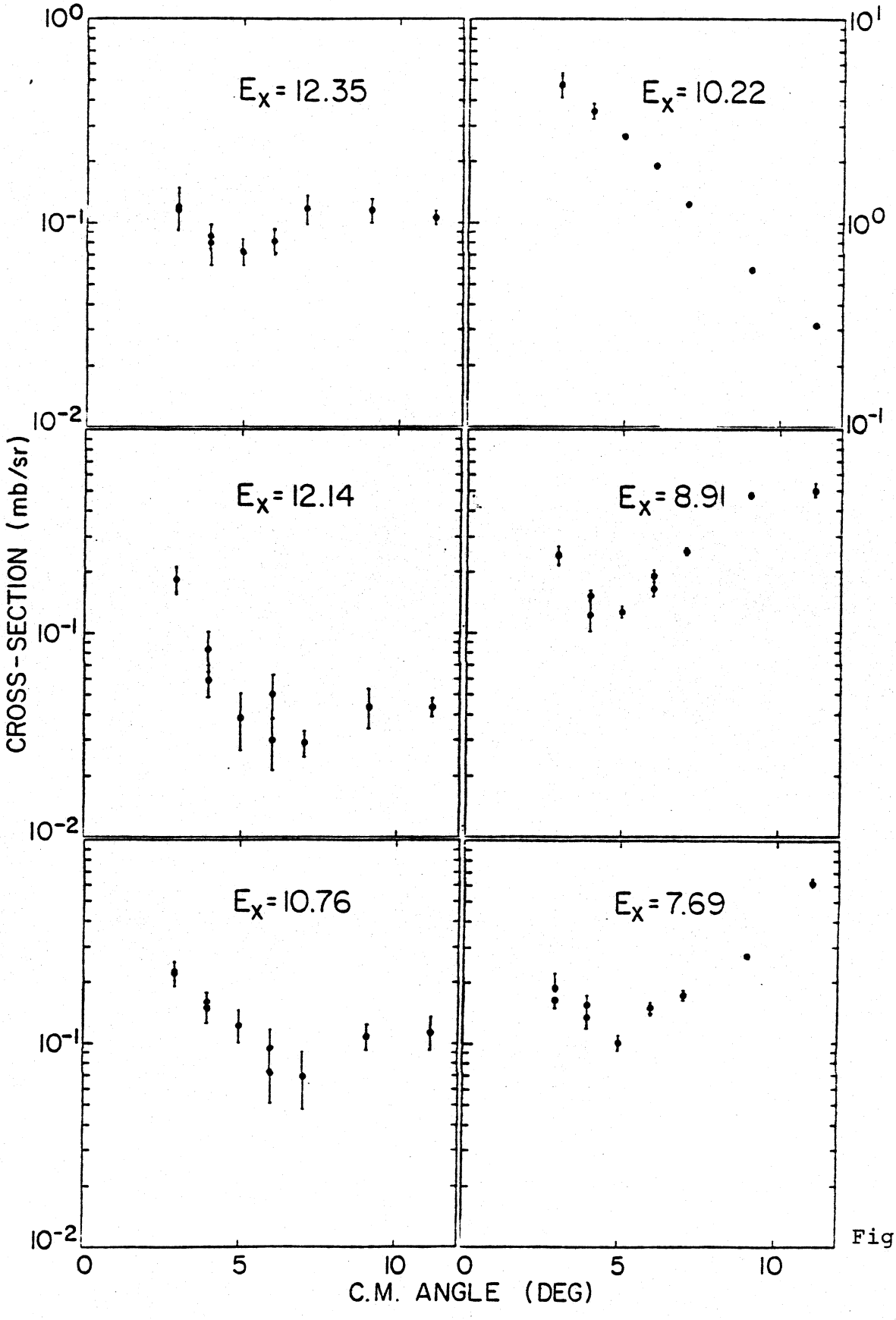
E_x = 12.35
E_x = 10.22
E_x = 12.14
E_x = 8.91
E_x = 10.76
E_x = 7.69
CROSS-SECTION (mb/sr)
C.M. ANGLE (DEG)
10^0
10^{-1}
10^{-2}
10^1
0
5
10

Fig. 18

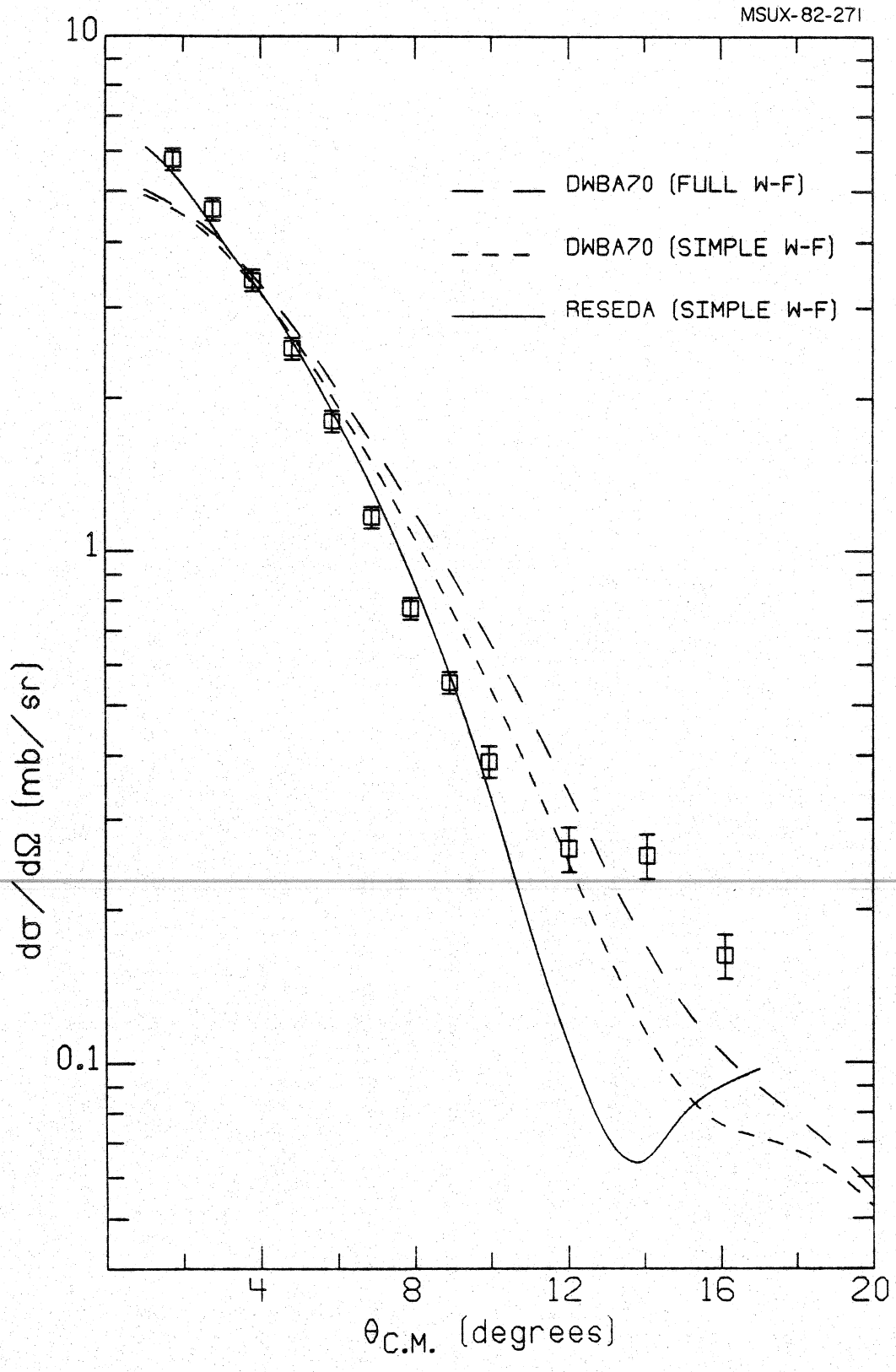
MSUX-82-271
10
1
0.1
4
8
12
16
20
DWBA70 (FULL W-F)
DWBA70 (SIMPLE W-F)
RESEDA (SIMPLE W-F)
dσ/dΩ (mb/sr)
θC.M. (degrees)

Fig. 19

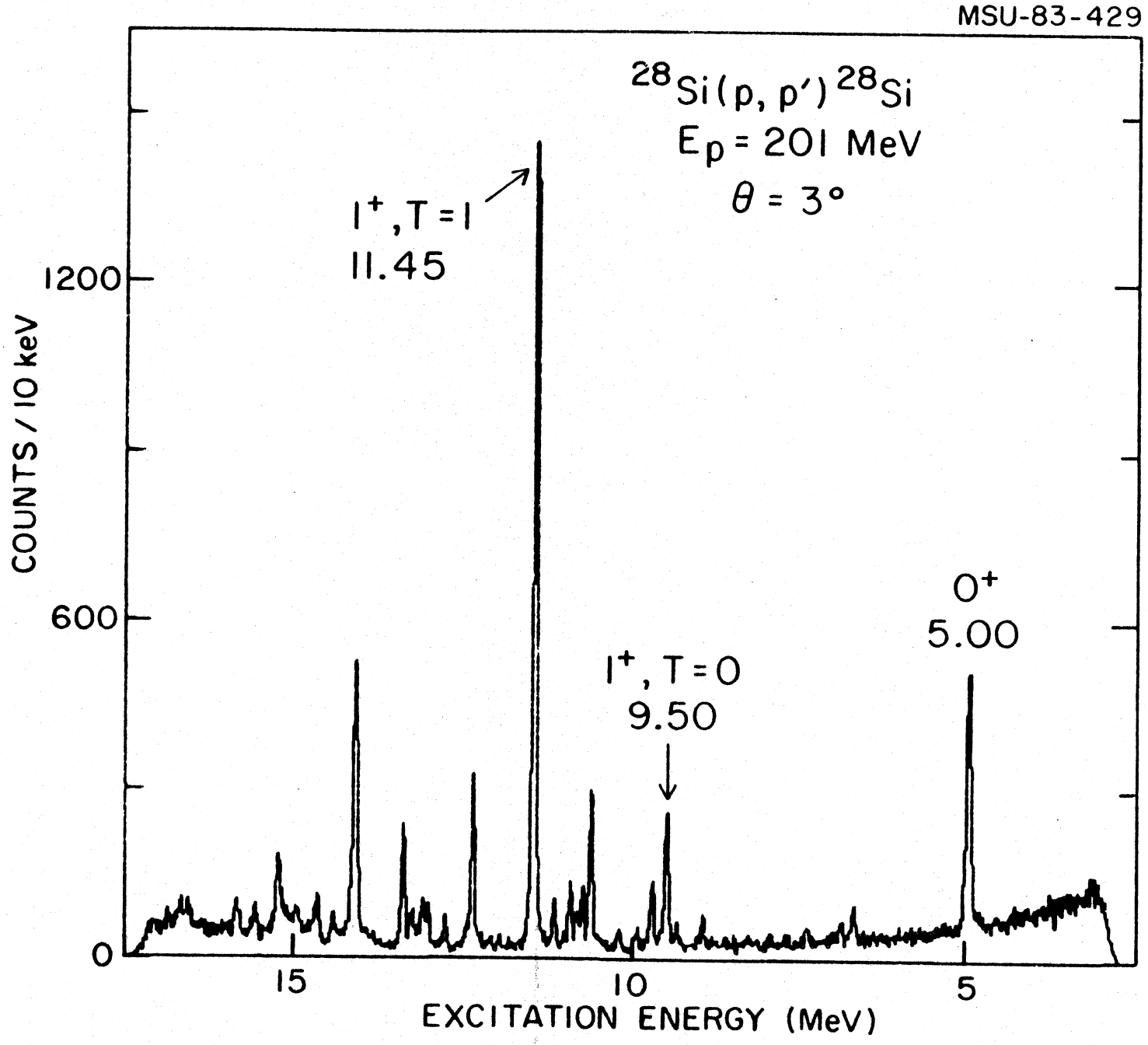
MSU-83-429
$^{28}Si(p, p')^{28}Si$
E_p = 201 MeV
θ = 3°
$1^+, T=1$
11.45
$1^+, T=0$
9.50
0^+
5.00
COUNTS / 10 keV
1200
600
0
15
10
5
EXCITATION ENERGY (MeV)

Fig. 20